THE UNIVERSITY OF
WARWICK

AUTHOR: **Peter P. Jones** DEGREE: **Ph.D.**

TITLE: **Determining Cluster-Cluster Aggregation Rate Kernels Using Inverse Methods**

DATE OF DEPOSIT: .....

I agree that this thesis shall be available in accordance with the regulations governing the University of Warwick theses.

I agree that the summary of this thesis may be submitted for publication.

I **agree** that the thesis may be photocopied (single copies for study purposes only).

Theses with no restriction on photocopying will also be made available to the British Library for microfilming. The British Library may supply copies to individuals or libraries. subject to a statement from them that the copy is supplied for non-publishing purposes. All copies supplied by the British Library will carry the following statement:

> "Attention is drawn to the fact that the copyright of this thesis rests with its author. This copy of the thesis has been supplied on the condition that anyone who consults it is understood to recognise that its copyright rests with its author and that no quotation from the thesis and no information derived from it may be published without the author's written consent."

AUTHOR'S SIGNATURE: .....

---

USER'S DECLARATION

1. I undertake not to quote or make use of any information from this thesis without making acknowledgement to the author.
2. I further undertake to allow no-one else to use this thesis while it is in my care.

DATE SIGNATURE ADDRESS

.....

.....

.....

.....

.....

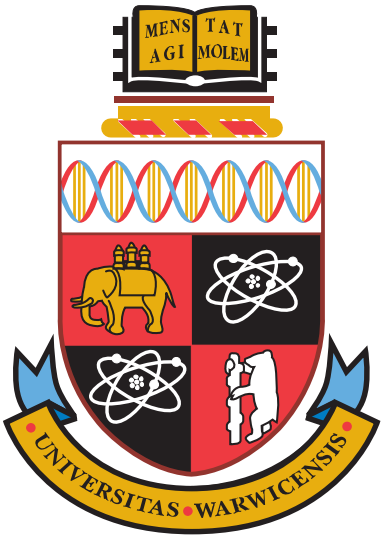


# Determining Cluster-Cluster Aggregation Rate Kernels Using Inverse Methods

by

**Peter P. Jones**

**Thesis**

Submitted to the University of Warwick

for the degree of

**Doctor of Philosophy**

**Theoretical Physics and Complexity Science**

July 2013

THE UNIVERSITY OF WARWICK

# Contents

# List of Figures

# List of Tables

# Acknowledgments

I would like to express profound gratitude to the following entities and individuals. To the EPSRC for the funding, and to the University of Warwick for being a wonderful institution. To Prof. Robin Ball, for the initial opportunity and ongoing support of the project. To Dr. Colm Connaughton for the excellent guidance and support provided throughout. To the remarkable Complexity Science DTC administrators, Phil Richardson, Monica Lucena, and Jen Bowskill, who made everything seem so seamless on the surface. Especially to Monica, who helped to smooth out the first few years of the ups and downs of the PhD process with a unique mixture of spirit and magnanimity. To friends, colleagues, and staff in the DTC and the Warwick Maths Institute, for being brilliant. To my family, for always being there. To anyone else who made the slightest contribution to helping this project along. Many thanks to one and all.

# Declarations

To the best of this author's knowledge the text of this thesis is entirely the work of its author except where otherwise indicated. The following are precise attributions regarding thesis content, including references to earlier texts by the author.

- Some text in the abstract and introductory chapter may have appeared earlier on the author's university webpage, in the online document "Determining Cluster-Cluster Aggregation Rate Kernels Using Inverse Methods: A Brief Non–mathematical Introduction to this Research for the Uninitiated" available via that webpage, and in contributions to prior papers mentioned below. At the time of thesis publication the webpage is at

  http://www2.warwick.ac.uk/fac/cross_fac/complexity/people/students/dtc/students2007/peterjones

- The incidental discovery (mentioned in Chapter 3), that significant oscillations persist in the presence of noise under certain nonlocal parameterisations of the finite size aggregation problem with source, was made by the author during the course of this research. It was investigated further in the multi-author paper (led by Connaughton) published as Ball et al. [2012].

- During this research, the author also made the incidental discovery (also mentioned in Chapter 3) that for certain finite system size Monte Carlo integrations of the aggregation problem with source the stationary distribution in the nonlocal regime perturbed by noise exhibits a quasicycle.

- The initial sets of exact distribution data used during the research in Chapter 4 were supplied by Connaughton.
- The paper Connaughton and Jones [2011] was based upon the work undertaken in Chapter 4.
- The novel regularisation function used in Connaughton and Jones [2011] and mentioned in Chapter 4 was discovered by the author.
- The novel inverse method in Chapter 5 is a joint construction by Ball, Connaughton, and the author. The research investigating the actual properties of the method, and the refinements and adaptations resulting therefrom are the work of this author. At the time of writing, a preprint paper based on the work is available at

  http://www.arxiv.org/abs/1301.4863

# Abstract

We investigate the potential of inverse methods for retrieving adequate information about the rate kernel functions of cluster-cluster aggregation processes from mass density distribution data. Since many of the classical physical kernels have fractional order exponents the ability of an inverse method to appropriately represent such functions is a key concern. In early chapters, the properties of the Smoluchowski Coagulation Equation and its simulation using Monte Carlo techniques are introduced. Two key discoveries made using the Monte Carlo simulations are briefly reported. First, that for a range of nonlocal solutions of finite mass spectrum aggregation systems with a source of mass injection, collective oscillations of the solution can persist indefinitely despite the presence of significant noise. Second, that for similar finite mass spectrum systems with (deterministic) stable, but sensitive, nonlocal stationary solutions, the presence of noise in the system can give rise to behaviour indicative of phase-remembering, noise-driven quasicycles. The main research material on inverse methods is then presented in two subsequent chapters. The first of these chapters investigates the capacity of an existing inverse method in respect of the concerns about fractional order exponents in homogeneous kernels. The second chapter then introduces a new more powerful nonlinear inverse method, based upon a novel factorisation of homogeneous kernels, whose properties are assessed in respect of both stationary and scaling mass distribution data inputs.

# Chapter 1

# Introduction

## 1.1 Prelude

An inverse problem is usually the data-driven complement of an existing theoretical forward problem. In a forward problem, we have investigated a physical phenomenon that we think we have a good theoretical model for, and have obtained experimental data. The task is to implement the model, compare the data that it produces with the experimental data, and to explain the differences, if any. With an inverse problem typically there is only a rough idea of what the model should be for some given phenomenon, and values of key parameters in the model are unknown. Given experimental data for the real phenomenon, the inverse problem is the attempt to determine the values of the key model parameters from the data[1]. If the data is sufficiently complete this task is relatively easy. But if the data is sparse or contains noise, then matters become more difficult.

[1] Asserting that there is a real distinction between inverse problems and parameter estimation problems is perhaps a matter of judgements about optimality of methods. If, in a particular problem, there is some functional relationship between the unknowns that can be exploited to reduce the problem to one of estimating a few parameters within that function, then the inverse problem of determining all the unknowns gets reduced to a parameter estimation problem. But if the same methods for seeking solutions still apply, the parameter estimation problem is still a member of the class of inverse problems.

In this thesis we deal specifically with a class of inverse problems concerning cluster-cluster aggregation (CCA). A basic description of the process involved in CCA is given by the following case. Imagine some oil mixed with water; two liquids that are immiscible in the same container. Also imagine that the mixture has been thoroughly stirred so that there are many very small globules of oil, of roughly equal size, evenly distributed throughout the water. Then we leave the mixture alone, and allow the currents within the fluid to bring oil globules together here and there as time passes. Typically, when two oil globules of masses $m_1$ and $m_2$ come into contact with each other they will merge to form a larger globule of mass $m = m_1 + m_2$. Mass is conserved in this merger process, so the mass of the large globule is equal to the sum of the masses of the two contributing globules.

For such a system the total pattern of mergers can be considered to be physically irreversible, in the sense that the likelihood of the large globule of mass $m$ spontaneously decomposing into two globules with precisely the masses $m_1$ and $m_2$ at some future time (before other events overtake matters) is small, and for the entire system of mergers, the entire reverse process that returns everything to its initial conditions has infinitesimal likelihood. In broad physical terms, these small probabilities of the reversal are because some kinetic or potential energy is dissipated during the process of aggregation and at the microscale the space of configurations is huge and changing, so the chances of energy being returned in precisely the way needed to reverse the aggregation neatly are very slight (and may even be zero). Types of system where irreversible bonding is a physical fact are obviously irreversible in this way.

In other aggregation processes the masses might also have geometric structure, like grains of sand, molecules or pollen, and instead of merging into a bigger blob, they aggregate to form larger clusters with spatial structure. Clusters can, of course, aggregate with other clusters; and although clusters can have spatial structure, in physics we can deliberately

overlook this should we choose to if we can argue for deliberately making some averaging approximation to simplify our models. If this is done, then we could treat the clusters as being effectively pointlike with all the details of geometry being averaged away. This is one aspect that distinguishes the process of cluster-cluster aggregation (CCA) from, for example, diffusion limited aggregation (DLA). (In DLA the object of study is the formation of a cluster from the accumulation of lone small masses over time - e.g. water molecules joining a snowflake under freezing conditions - and the study of the resulting cluster structures is a prominent concern.)

We might also imagine that the process of merger between globules could happen (statistically, averaging over a large number of mergers) at a rate dependent on the magnitudes of two contributing masses. For example, if there is a very large globule in a sea of very small globules then we might expect mergers between the large globule and small globules to happen at a faster rate than mergers between small globules, simply because the large globule occupies more space and constitutes a bigger target as the mixture swirls. However, in another completely different mixture, mergers between large and small globules might be less likely, and hence happen at a slower rate, because of chemical, electrostatic, or hydrodynamic interferences.

Research in cluster-cluster aggregation has progressed for a long time using a model based on the Smoluchowski Coagulation Equation (SCE) [Smoluchowski, 1917]. It has been used to successfully model aggregation, coagulation, and coalescence processes that abound in nature and span all scales, ranging from the microscopic scales of atmospheric aerosol formation [Friedlander, 1977], to the cosmological scales of the clustering of matter within the universe [Silk and White, 1978]. The effectiveness of the SCE relies on a number of assumptions that are, in effect, averaging approximations: well-mixed, very large systems; spatial uniformity of processes; mixtures sufficiently dilute that only pair-

wise interactions between particles are likely. That is, the SCE states that the mean number of masses $N(m,t)$ (per unit of volume) of mass $m$ present at some time $t$, averaged over suitably sized regions within the mixture, is a function of the similarly spatially-averaged rates at which other pairs of masses present can clump together to form a mass of size $m$, minus the spatially-averaged rates at which masses of size $m$ might join with other masses. Our ability to apply averaging assumptions to the problem places the SCE in the class of so-called mean-field approximations, which are valid only if we can average over a sufficiently large number of interactions to be able to talk sensibly about the changes in number density $N(m,t)$ being independent from spatial correlations. This translates into being able to assume that the density of pairs of masses factorises at all times $t > 0$, such that,

$$N^{(2)}(m_1,m_2,t) \propto N(m_1,t)N(m_2,t) \tag{1.1}$$

Under this mean-field assumption, the system of equations represented by the SCE exhibits closure, with changes in concentrations depending only upon other concentrations (first-order densities) and not upon an entire hierarchy of product density functions,

$$N^{(2)}(m_1,m_2,t), N^{(3)}(m_1,m_2,m_3,t), ..., \tag{1.2}$$

An advantage of the SCE is that it is the simplest effective description of an aggregating system. However, there are also some snags with the SCE. One is that many real systems are not vast and internally they exhibit (statistical) spatial heterogeneities - for example if large masses hoover up all smaller masses in their immediate neighbourhood creating ‘moats’ of empty liquid around them - so the averaging can break down. Another snag is that even in the comparatively simple general case of an aggregation process without a constant source

of injected mass, analytic solutions for the evolution of the distributions of mass sizes over time are known for only a few special aggregation rate kernel functions. Hence, in general, there is both the forward problem of predicting the likely outcome of using some other kernel function in some process, and the inverse problem of inferring kernels from observed data for the mass (density) distribution $N(m,t)$. Computer simulations of aggregation can be made for specific forward problems, but it is excessively time-consuming to attempt to find which kernel matches a particular mass distribution by simulating all parameterisations of some subset of all classes of possible kernels. Hence the efforts to find effective, efficient inverse methods.

## 1.2 The Contemporary Relevance of the Inverse Problem

A particular example that is of strong contemporary interest is the role played by droplet coalescence in cloud formation and the clouds' internal dynamics. A better understanding of this process would improve the precision of climate evolution projections [Stephens, 2005].

However, considering real aggregation systems like the formation of raindrops, turbulence in the supporting medium (the cloud air mass) complicates the task significantly. It may have a non-trivial role in determining the collision rate of water droplets [Bodenschatz et al., 2010][Grabowski and Wang, 2009]. Moreover, it seems likely that turbulence at larger scales interacts strongly with the micro-physics of the rain formation process. Coupling the macro- and microscopic scales of simulation of weather systems remains a significant computational challenge. While small-volume direct numerical simulation of droplets in turbulent flows [Reade and Collins, 2000][Wang et al., 2008] are possible, it is not yet clear whether these simulations adequately represent the true turbulent conditions acting upon rain formation within a cloud.

Complete theoretical description of the statistical interplay between particles and turbulence also remains elusive. However, owing to recent technological advances, both the quality and quantity of empirical data obtained from observations have significantly increased [Siebert et al., 2006]. It therefore makes sense to explore using inverse methods upon this data as means to obtain useful insights. The use of inverse methods can also provide additional quantitative measures for optimising the choice of model in contexts in which the microphysics is unknown or controversial.

The inverse problem which we discuss in this thesis is to extract the functional form of the mass-dependent coalescence rates[2], $K(m_1, m_2)$, given the measurements of the time evolution of the droplet size distribution, $N(m,t)$. Prior methods for this problem are found in Wright and Ramkrishna [1992] and Onishi et al. [2011]. (Wright and Ramkrishna [1992] is the most general development from precursors in Muralidhar and Ramkrishna [1986], Muralidhar and Ramkrishna [1989], Wright et al. [1990], Wright et al. [1992]. Onishi et al. [2011] extends developments in Onishi et al. [2008].) In Onishi et al. [2011] the method does not depend upon self-similarity of $N(m,t)$ but significant prior knowledge about droplet coalescence in turbulent conditions was used to put strong constraints on the functional form of the kernel, thus simplifying the inversion problem at the expense of a loss of generality. The method in Wright and Ramkrishna [1992], for use with self-similar decay case distributions, does not strongly constrain the kernel form, but the paper only treated example kernels with homogeneity exponents[3], $\lambda \in \{0, 1\}$.

In this thesis we demonstrate that a weakness of the Wright and Ramkrishna [1992] method is that it does not retrieve kernel functions containing fractional order exponents sufficiently well. We then provide a new inverse method which assumes only kernel homogeneity and yet exhibits powerful new capabilities in respect of the inverse problem under

[2] For its mathematical role within the SCE this function is also called a kernel function.
[3] See equation (2.5) for the definition of the kernel homogeneity exponent $\lambda$.

consideration. For a broad class of kernel functions, we demonstrate that our method will retrieve good representations of kernels from the main forms of distribution data. (See Chapter 2 for more details about the forms of mass distributions, and Appendix B for some information about the kernel functions we used to generate test data sets).

## 1.3 Thesis Structure

In Chapter 2, the properties of the SCE are introduced, and we provide a brief overview of the different classes of solutions. Then in Chapter 3 simulation of the SCE using Monte Carlo techniques is discussed, and some incidental discoveries made using the Monte Carlo simulations are mentioned. The main research material is then presented in two subsequent chapters. Chapter 4 (see also Connaughton and Jones [2011]) investigates the capacity of method in Wright and Ramkrishna [1992] in respect of concerns about fractional order kernel exponents. In Chapter 5 we propose a novel and more powerful method whose properties are assessed in respect of the main forms of $N(m,t)$ mass distribution data.

## 1.4 A Note on Terminology

Throughout this thesis we will use the following (non-standard) terminological shorthand. When we refer to the *decay case* we mean a system that has an initial mass distribution, $N(m,0)$, but no constant source of injected mass. The system then evolves through aggregations taking place, and the mass distribution $N(m,t)$ "decays" until a single large mass remains. In the literature the decay case is usually described as "aggregation without source". Calling it the decay case in the text makes it easier to distinguish from the classes of "aggregation with source" that are also described later on.

# Chapter 2

# Cluster-Cluster Aggregation and the Smoluchowski Coagulation Equation

## 2.1 General Properties

For a large variety of aggregation phenomena the Smoluchowski Coagulation Equation (SCE) [Smoluchowski, 1917] gives a mean-field description of the evolution of the average concentrations, $N(m,t)$, of mass sizes $m$ per unit volume in a suitably large, dilute, and well-mixed, system of coalescing or aggregating masses in some supporting medium. A good example is chemical monomers with suitable bonding properties in suspension. The individual masses diffuse or are advected within the fluid and they collide, sticking together with some probability.

With respect to the study of clouds the utility of the SCE lies in approximating phenomena such as the formation of rain from smaller water droplets [Rogers and Yau, 1989], or study of the coagulation of dust or soot particles [Friedlander, 1977], such as those ejected into the atmosphere from desert winds, volcanic eruptions [Costa et al., 2010] or industrial smokestacks, in various atmospheric conditions. Moreover, atmospheric turbulence is

thought to play a role in the rate of formation of rain [Falkovich et al., 2002] (though the degree of influence remains a matter of some debate [Devenish et al., 2012]), and there is an analog of the SCE for the cascades of energy between different scales of turbulent eddies [Connaughton et al., 2006]. So the SCE would perhaps be expected to play a significant role in modelling droplet coagulation in a turbulent medium during the formation of rain.

Mathematically and in numerical simulation, the SCE can be approached as a deterministic system of integro-differential equations, or treated probabilistically as a Markov Process [Aldous, 1999][Bertoin, 2006]. We will not discuss the contents of the extensive probabilistic literature in detail here, except to mention the relevance of probabilistic theorems concerning convergence toward the mean-field solutions when considering the evolution of finite mass Monte Carlo simulations [Fournier and Giet, 2004] (see also Chapter 3).

In the discrete form of the SCE, all larger masses are taken to be multiples of a minimum (monomer) mass $m_0$, and by assuming a convenient rescaling we can take $m_0 = 1$. The SCE asserts that the rate of change of the concentration, $N_m(t) = N(m,t)$, for any $m \in \mathbb{N}$, evolves according to:

$$\frac{\partial N(m,t)}{\partial t} = \frac{1}{2}\sum_{m_1=1}^{m-1} K(m-m_1,m_1)N_{m-m_1}(t)N_{m_1}(t) - \sum_{m_1=1}^{\infty} K(m,m_1)N_m(t)N_{m_1}(t) + J\delta(m-1) \tag{2.1}$$

The first sum on the right hand side of (2.1) represents the total rate at which two smaller mass combine to form masses of size $m$. The second sum represents the total rate at which masses of size $m$ combine with other masses to make masses larger than size $m$. Typically, they are called the gain and loss terms, respectively, for $N(m,t)$. The binary symmetric mass-dependent kernel function, $K(m_1,m_2)$, is used to capture all the information about the

average rates at which two masses $m_1$ and $m_2$ could meet and coalesce. In the decay case of aggregation without a constant source of injected mass, the rate of mass injection is $J = 0$. When there is a source injecting mass into the system, then $J > 0$.

For systems constrained to have a finite spectrum of mass sizes the upper limit on the second sum can be a finite maximum mass size $M < \infty$. Even if the upper limit of the second sum term is less than infinity, such a finite mass size version of the discrete SCE can remain valid as a mean-field approximation to that system, assuming an absence of spatial correlations (on the relevant timescale of observation). Extra terms can be added to such versions of the SCE depending on whether the masses larger than $M$ are counted within total mass conservation, or lost outside the system. If $L_M(m)$ represents the masses larger than $M$ one can write,

$$\frac{\partial N(m,t)}{\partial t} = \frac{1}{2}\sum_{m_1=1}^{m-1} K(m-m_1,m_1)N_{m-m_1}(t)N_{m_1}(t) - \sum_{m_1=1}^{M-m} K(m,m_1)N_m(t)N_{m_1}(t) + J\delta(m-1) - L_M(m,t) \tag{2.2}$$

$$L_M(m,t) = \sum_{m_1=M-m+1}^{M} K(m,m_1)N_m(t)N_{m_1}(t) \tag{2.3}$$

Irrespective of whether the system has an upper mass size limit or not, when the mass spectrum is continuous, then the SCE has an equivalent continuous form (sometimes attributed to Müller [1928]) as shown in (2.4). In this case there can be interesting discussions in mathematical treatments about how small $m_0$ must be (see, for example, the discussion of 'dust' in Bertoin [2006], Escobedo and Mischler [2006]).

$$\frac{\partial N(m,t)}{\partial t} = \frac{1}{2}\int_0^m K(m-m_1,m_1)N(m-m_1,t)N(m_1,t)dm_1 \\ -\int_0^\infty K(m,m_1)N(m,t)N(m_1,t)dm_1 + \frac{J}{m_0}\delta(m-m_0) \tag{2.4}$$

The assumption of the lack of spatial correlations, averaged over an appropriate timescale, is the basis for the SCE's mean-field validity. This spatial homogeneity means that in systems where the rates of transport, or of collisions, are presumed to be sufficient to overcome prolonged spatial inhomogeneities, a single point average is effectively representative of the entire system. Hence the lack of spatial parameters in (2.1) and (2.4).

In the basic case, aggregation is assumed to be irreversible and aggregates do not fragment. Given some initial mass distribution, $N(m_0,0)$, and a particular (bounded) function for $K(m_1,m_2)$, the SCE provides the evolution of the mass distribution $N(m,t)$ for all mass sizes $m$ for times $t > 0$.

## 2.2 Decay Case Distributions

Decay case distributions are those where an initial input of masses, $N(m_0,0)$, at time $t = 0$ is then allowed to evolve without there being further injections of mass. In the subgelation regime (discussed briefly later in §2.2.2), given a finite initial input $N(m_0,0) = I_0$ the system will evolve over time to a single largest mass $M = I_0$. Even in the comparatively simple decay case, analytic solutions of the SCE for $N(m,t)$ are known only for a limited set of kernels, including the classic set $K(m_1,m_2) \in \{1, m_1+m_2, m_1m_2\}$ (see Krapivsky et al. [2010], Davies et al. [1999], Wattis [2006], Leyvraz [2003] and references therein) and their linear combination [Spouge, 1983a,b].

On the positive side, since the analytic solutions for the classical cases $K(m_1, m_2) \in \{1, m_1 + m_2, m_1 m_2\}$ are known, these can be used to calibrate numerical simulations of the SCE (see Chapter 3). A list of the (discrete and continuous) solutions for these classical kernels can be found in [Aldous, 1999, Table 2]. Modern derivations of these solutions (for the discrete SCE) found using generating functions can be found in Krapivsky et al. [2010] and Wattis [2006]. For the continuous SCE, the generating functions are replaced by their continuous counterpart, the Laplace transform.

Considering the decay case for arbitrary kernels, while it is known that for suitable initial conditions the SCE has a unique solution, it has also been shown that in general (for any possible initial conditions) solutions of the SCE need not be unique for a given kernel [Norris, 1999]. Even if a single kernel function $K(m_1, m_2)$ is capable of producing more than one consistent solution, then this still might not present a problem when inverting from data to determine the kernel. What matters for the purposes of the inverse problem is whether a given distribution $N(m,t)$ has a unique kernel, and because the mean-field SCE is a deterministic differential equation this is true, provided one can make assumptions that the spread of possible initial conditions is not too broad.

A key consideration that can help to constrain the breadth of the class of initial conditions, is to restrict discussion to the class of physically feasible aggregations. It has been suggested that kernel functions of physical interest are typically homogeneous functions of their arguments [Kang et al., 1986]. This is because more realistic kernels often yield homogeneous kernels in particular limits.

The degree of homogeneity, $\lambda$, of such kernels is defined by the relation,

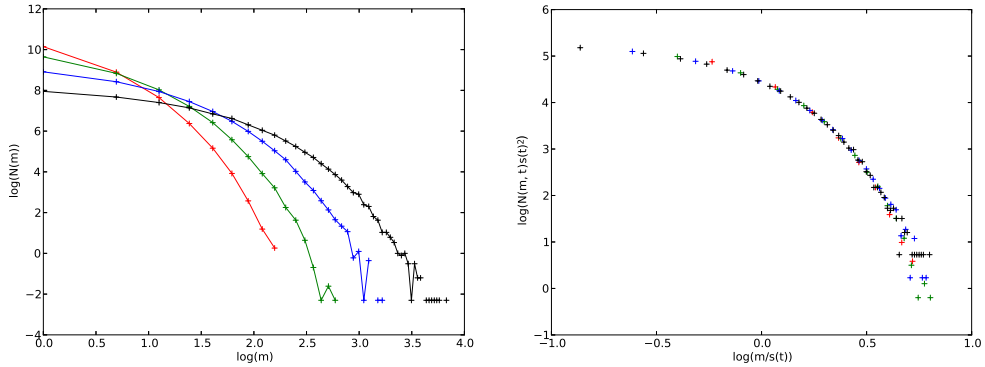


Figure 2.1: The left image shows the evolution in time of the mass distribution for the constant kernel $K = 1$ which has degree of homogeneity $\lambda = 0$. Each curve is an average from 10 runs simulated using the Monte Carlo method for discrete mass with a maximum mass size cutoff of $M = 300$. The lines shown are solely for illustrative purposes. The fluctuations as $\log(m)$ increases are partly the result of low concentrations of large masses in a system of this size, and partly because of masses larger than $M = 300$ leaving the system. The right image shows the result of applying rescaling to produce the time-independent scaling distribution.

$$K(hm_1, hm_2) = h^{\lambda} K(m_1, m_2) \tag{2.5}$$

### 2.2.1 Scaling Decay Case Distributions

For most homogeneous kernels, the evolution of the mass distribution is typically self-similar and scaling arguments for $N(m,t)$, as reviewed in Leyvraz [2003], can also be applied to create some mathematical simplification by mapping $N(m,\cdot) \to \Phi(z)$, with $\Phi(z)$ being a time-independent distribution curve, as shown in Figure 2.1. The mapping takes the form,

$$N(m,t) \sim s(t)^{-\tau} \Phi(z) \qquad z = \frac{m}{s(t)} \tag{2.6}$$

where $s(t)$ is the typical cluster size. This can be defined as a ratio of moments of the size distribution [Leyvraz, 2003][Wright and Ramkrishna, 1992]. The moments are defined as:

$$\mathscr{M}_n(t) = \int_0^\infty m^n N(m,t)\, dm \tag{2.7}$$

Then, provided mass is conserved during the evolution of the system, the following equation provides a valid way to extract the evolution of the scaling typical mass from the distribution data.

$$s(t) = \frac{\mathscr{M}_2(t)}{\mathscr{M}_1(t)} \tag{2.8}$$

Knowledge of $s(t)$ can then be used to obtain the scaling function, $\Phi(z)$. As it is time-invariant, $\Phi(z)$ can be considered to determine the shape of the mass distribution.

For decay case systems it can be shown that $\tau = 2$ as long as the second moment of the system $\mathscr{M}_2 < \infty$ for all times (see e.g. van Dongen and Ernst [1988]). Although the scaling function is not fully understood it is known that the large $z$ behaviour is of the form $\Phi(z) \sim e^{-\beta z}$ [Krapivsky et al., 2010, p.155] and in some cases, for practical purposes, it is considered to be well matched in that regime by a sum of Gamma distributions [Wright and Ramkrishna, 1992][Goodisman and Chaiken, 2006]. However, for some kernels this is not true, and for the purposes of obtaining a suitably continuous function to use in inversion, resorting to approximation using (automated fitting of) piecewise interpolations can be necessary.

Scaling (or self-similar) solutions for the classical kernels are also known [Connaughton et al., 2009][Leyvraz, 2003][Menon and Pego, 2004][Menon and Pego, 2006]

[Menon and Pego, 2008], and a great deal is known about the scaling solutions for homogeneous kernels in general [van Dongen and Ernst, 1988][Davies et al., 1999][Leyvraz, 2003][Fournier and Laurençot, 2005][Goodisman and Chaiken, 2006]. Scaling arguments allow for the deduction of properties (typically information about the values of key exponents) of general solutions to the SCE at large times and large masses [van Dongen and Ernst, 1988][Leyvraz, 2003]. Usually the scaling limit is defined to be the set of conditions: $t \to \infty$, $m \to \infty$ but with the ratio $m/s(t)$ kept fixed and finite.

As noted in Leyvraz [2003] the range of solutions to which these arguments apply depends on subtleties of how one defines scaling, with strong or weak notions of convergence. The mathematical existence of a large class of scaling solutions is shown in Fournier and Laurençot [2005]. A counter to the problem of broad initial conditions follows for the classical kernels $K(m_1, m_2) \in \{1, m_1 + m_2, m_1 m_2\}$ from proof that solutions with exponential tails attract all solutions with finite $(\lambda + 1)^{\text{th}}$ moment [Menon and Pego, 2004] in the regime of large times required by scaling arguments. In Leyvraz [2003] it is asserted that for a suitable notion of *weak convergence*, scaling of the solution holds 'under all reasonable circumstances' (i.e. the class of initial conditions is adequately broad).

Scaling distributions have an obvious advantage over the time–dependent distributions in that only a few time snapshots are required to demonstrate that scaling is applicable, and hence the data collection requirements are more in alignment with contemporary real collection capabilities. Since the homogeneous kernels that give rise to scaling solutions are also time-independent functions, scaling distributions still contain enough information to enable inference of key kernel properties. Although for finite size systems the scaling hypothesis only holds approximately, in many cases the rescaling collapse approximates a single curve sufficiently well to consider its use in inverse methods.

### 2.2.2 Gelation

It can be demonstrated that for infinite systems and homogeneous kernels with $\lambda \geq 1$ (e.g. $K(m_1, m_2) = m_1 m_2$) that the aggregating system will undergo a transition called gelation within a finite time. At the critical time $t_c < \infty$ the second moment of the mass distribution diverges. It can even happen that $t_c = 0$ in the instantaneously gelling case. An interpretation of this is that a single mass (called the gel) of infinite size is formed. See Krapivsky et al. [2010] for an introduction to these issues, Lushnikov [2006] for a review with a probabilistic viewpoint, and Ball et al. [2011] for an insightful contemporary update especially concerning finite system size effects, and the references therein.

Since treatment of the inverse problem for decay case systems with gelation is beyond the scope of this thesis, we will not discuss those further here. However, our new inversion method presented in Chapter 5 does treat the finite mass spectrum stationary distributions for kernels that would be gelling kernels in the infinite mass spectrum decay case.

## 2.3 Stationary Distributions

Stationary distributions arise when there is a constant injection of small masses into the system, with $J > 0$ (typically normalised to be $J = 1$), and a finite upper mass size cutoff, $M$, beyond which masses leave the system. Under these conditions, eventually the rate of change of the concentrations tends to zero, $\partial_t N(m,t) = 0$, and the solution of the SCE is time-independent, as $N(m)$.

### 2.3.1 Local and Nonlocal Regimes

Before discussing the forms of distributions it is worth noting that in the theoretical literature the homogeneity exponent $\lambda$ of the kernel is often considered to be composed as

$\mu + \nu = \lambda$ [van Dongen and Ernst, 1988][Lee, 2000], where $\mu$ and $\nu$ relate to the asymptotic properties of the kernel at very large masses, $K(m_1, m_2) \sim m_1^{\mu} m_2^{\nu}$ with $m_2 \gg m_1$ and typically with $\nu > \mu$ and $\nu < 1$. Without going into too much detail at this stage, (in the non-gelling regime) a distinction is made between a *local* regime where the asymptotic behaviours of the mass distributions are independent of the upper mass size as $M \to \infty$, and the *nonlocal* regime where a dependence upon increasing $M$ is retained. For formal reasons relating to relevant equations these two regimes are characterised by $|\nu - \mu| < 1$ (local) and $|\nu - \mu| > 1$ (nonlocal) respectively, but the intuitive explanation is that in the nonlocal regime there remains a strong flux relationship between (very) small and (very) large masses as $M$ increases towards infinity [Ball et al., 2012][Connaughton et al., 2004][Connaughton et al., 2008].

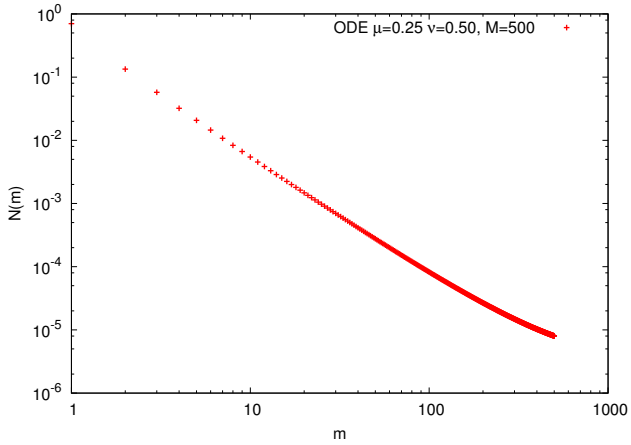


Figure 2.2: A local regime stationary distribution generated using ODE integration of the SCE for the kernel $K(m_1, m_2) = \frac{1}{2}(m_1^{\mu} m_2^{\nu} + m_2^{\mu} m_1^{\nu})$, with $(\mu, \nu) = (0.25, 0.50)$, $J = 1$, and $M = 500$.

In the local regime the stationary states are found to be stable for a class of kernels (see Krapivsky and Connaughton [2012], Hendriks and Ziff [1985], Crump and Seinfeld [1982], White [1982]) whose form becomes fully independent of $M$ as $M \to \infty$. That is, any effect $M$ has upon the form of the mass distribution is confined to being close to $M$. In the nonlocal

regime, the aforementioned relationship between the parameterisation of the kernel and the upper mass size cutoff determines whether the mass distribution is stable or manifests non-stationary dynamical behaviour [Ball et al., 2012] (and c.f. Krapivsky and Connaughton [2012]).

For suitable kernels, the mass distribution in the local regime forms a power law for small to medium size masses, but has an exponential tail at large masses. The general form of $N(m)$ for arbitrary kernels was determined in Connaughton et al. [2004], and is given by:

$$N(m) \sim \sqrt{J} m^{-\frac{(\mu+\nu+3)}{2}} \tag{2.9}$$

The exponent $-(\mu+\nu+3)/2$ implies that there is a constant flux of mass through increasing mass sizes [Connaughton et al., 2008]. Hence such states are classic examples of non-equilibrium stationary states with a conserved current [Ball et al., 2012].

An asymptotic (for large $M$) approximation to the form of $N(m)$ in the nonlocal regime, valid for medium to large mass sizes, was recently derived in Ball et al. [2012] (drawing on earlier specific work in Horvai et al. [2008]) and is shown below.

$$N^*(m) \sim \sqrt{2\zeta J \log(M)} M^{-1} M^{m^{-\zeta}} m^{-\nu} \tag{2.10}$$

Here, $\zeta = \nu - \mu - 1$ with the convention that $\nu > \mu$. As is noted in Ball et al. [2012], this formula implies that the stationary state vanishes as $M \to \infty$. It is demonstrated in Ball et al. [2012] that for a range of parameterisations in the nonlocal regime, the stationary states are unstable, and the dependency upon $M$ manifests as substantial, sustained, periodic oscillations in the mass flux for a range of values of $M$.

Some prerequisites for being able to apply inverse methods successfully with such finite mass distributions with an injection source are therefore that either the distribution be found to be stationary (over sufficient time), or that sufficient data is available to construct a pseudo-stationary distribution by estimating the discounting for any flux oscillations.

### 2.3.2 Time-Dependent Growth of Stationary Distributions

A trivial scaling for time-dependent growth of a stationary distribution can arise when there is a constant injection of small masses into the system and a very large upper mass size cutoff beyond which masses leave the system. That is, $M \to \infty$. This behaviour is depicted Figure 2.3. Rescaling with respect to the evolution of the typical mass $s(t)$ of the system will recover the associated final stationary distribution. In this thesis we do not attempt to apply inverse methods to transient evolutions of the mass distributions such as these, although it is likely that the new methods developed in Chapter 5 could be applied.

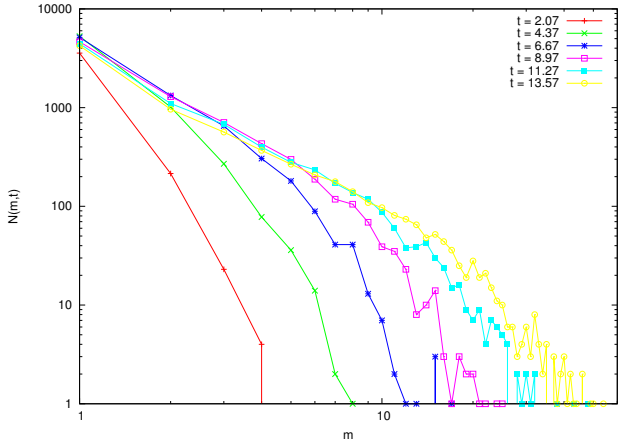


Figure 2.3: A Monte Carlo simulation exhibiting a growing stationary distribution for the kernel $K(m_1,m_2) = \gamma\frac{1}{2}(m_1^{\mu}m_2^{\nu} + m_2^{\mu}m_1^{\nu})$, with $(\mu,\nu) = (-0.25, 0.50)$ and $\gamma = \frac{1}{20000}$, evolving in time when the upper cutoff mass size is large. In this case $M = 1000$, and the Monte Carlo simulation injection rate is $J_{\mathrm{MC}} = 2000$.

## 2.4 Non-stationary, Non-scaling Distributions

Lastly, we mention that for real clouds, rain formation is thought also to involve some measure of fragmentation of droplets, as collisions at sufficient relative velocity cause some break-up of the drops. In theory, depending upon the extent of fragmentation assumed for a system the $N(m,t)$ can eventually reach a steady state, as mass is recycled from larger to smaller sizes. However, it is suggested that the durations required for steady states to form are too long compared with real rain formation (except in the case of heavy rainfall) [Prat and Barros, 2007]. So it is possible that data from measurements of real clouds could represent transient distributions.

A key question is whether these transient distributions exhibit scaling for some portion of the mass distributions. If they do, then it might be possible to model at least part of their behaviour using a kernel function of some degree of homogeneity. Otherwise inverse methods that fully track both mass and time will be required.

# Chapter 3

# Monte Carlo Simulation

## 3.1 Monte Carlo Simulation of Cluster-Cluster Aggregation

In order to simulate the SCE, we made use of a method for the Monte Carlo (MC) simulation of chemical mixing introduced in Gillespie [1976]. The full method in Gillespie [1976] is designed to cope with coupled chemical reactions wherein a particular reaction might have the form:

$$S_1 + S_2 \xrightarrow{R(1,2)} 2S_3 \tag{3.1}$$

Here, the subscripts indicate different chemical types: two different chemicals react to provide two molecules of a third chemical at a rate governed by a function of the types, $R(1,2)$. For our simulations of cluster-cluster aggregation we are interested only in the conservation of mass as clusters composed of the same material merge. So a cluster of mass $i$ and a cluster of mass $j$ aggregate to form a cluster of mass $i+j$ at a rate governed by a function of the magnitudes of the masses, $K(i,j)$.

$$A_i + A_j \xrightarrow{K(i,j)} A_{i+j} \tag{3.2}$$

This simplified method is described in Connaughton et al. [2009] but we will repeat the salient points here. The Monte Carlo process simulates the aggregation process (described by the SCE) as a series of events. Each event is the aggregation of two masses. At time $t$, the probability $P(\hat{m}_1, \hat{m}_2, t)$ that an aggregation occurs between masses of two different sizes, $\hat{m}_1$ and $\hat{m}_2$, can be calculated according to:

$$P(\hat{m}_1, \hat{m}_2, t) = \frac{K(\hat{m}_1, \hat{m}_2) N(\hat{m}_1, t) N(\hat{m}_2, t)}{\sum_{\forall m_1, m_2} K(m_1, m_2) N(m_1, t) N(m_2, t)} \tag{3.3}$$

Where $N(m,t)$ represents the number of clusters of mass $m$ present at time $t$. An event is selected by forming the partial sums of the $P(m_1, m_2, t)$ and then choosing one by matching the partial sums to a uniform random number, $r$, generated on the interval $[0,1)$. The event indexed by $i = n+1$ is then selected by using,

$$\sum_{i=1}^{n} P_i(t) < r \leq \sum_{i=1}^{n+1} P_i(t) \tag{3.4}$$

Equivalently, if we have the set of interaction types $S = \{(m_1, m_2) : (m_1, m_2) \sim (m_2, m_1)\}$, where $(m_1, m_2) \sim (m_2, m_1)$ denotes equivalence because of the symmetry of the kernel function, then the total number of types of possible aggregation events is given by $N_A = \#S$ (where # is the set cardinality operator). We can then form the total rate,

$$R_{\text{tot}}(t) = \sum_{i=1}^{N_A} R_i(t) = \sum_{\forall(m_1,m_2)\in S} K(m_1,m_2)N(m_1,t)N(m_2,t) \tag{3.5}$$

The ordering of the sum over the pairs of mass sizes does not matter because $r$ is picked randomly. Then for some index integer $n \leq N_A$, it will be the case that,

$$\sum_{i=1}^{n} R_i(t) < R_{\text{tot}}(t)r \leq \sum_{i=1}^{n+1} R_i(t) \tag{3.6}$$

Thus the event indexed by $i = n+1$ will be selected as the next aggregation event.

To modify this process to cope with the case of aggregation with a source of monomer masses injected at rate $J$, we simply count mass injection as another event type and form,

$$R_{\text{tot}}(t) = J + \sum_{i=1}^{N_A} R_i(t) \tag{3.7}$$

The process of selecting which event type will occur next using $r$ is similarly modified.

The total rate (at a particular time), $R_{\text{tot}}(t)$, is used to parameterise the generation of an amount of time that elapses in the system when an aggregation takes place. More specifically, the event interarrival waiting times are given by sampling from an exponential distribution according to,

$$P(\Delta\hat{t}) = Re^{-R\Delta\hat{t}}, \qquad \text{where } R = R_{\text{tot}}(t) \tag{3.8}$$

This approach is valid because every aggregation event is considered to be an independent event, of a type that would occur (if repeated in time) with a mean rate given by, for example, $K(m_1,m_2)$ multiplied by the time-dependent product of the mass densities $N(m_1,t)N(m_2,t)$. Hence, as the system evolves, what changes over time in $R$ is the sum of the mean rates of the Poisson distributed events as a function of changes in the products $N(m_1,t)N(m_2,t)$ for each pair $(m_1,m_2)$.

In the evolution of the SCE, $N(m,t)$ is, strictly speaking, the mean-field average of the number of clusters of size $m$ considered over all locations in a suitably large spatial domain. However, physical particles moving through space do so at finite (diffusion or advection) velocities, taking time to transit from one place to another, whereas the MC simulation (as described above) is effectively zero-dimensional. Hence a tuning parameter must be added to compensate for the absence of spatial movements by particles in order to make the mean aggregation rates more realistic. The tuning parameter is in effect a suitable rescaling of time. Given this tuning parameter, $\gamma$, the rates above are reformed as,

$$R_{\text{tot}}(t) = J + \sum_{i=1}^{N_A} \gamma R_i(t) = J + \sum_{\forall(m_1,m_2)\in S} \gamma K(m_1,m_2)N(m_1,t)N(m_2,t) \tag{3.9}$$

Then the (suitably tuned) MC simulation will approximate the mean-field in two main ways. First, if a particular run of the simulator involves enough particles, then the Law of Large Numbers suggests that aggregation events will occur at rates approximating their mean rates. Secondly, an ensemble of runs can be averaged over to further improve the approximation of the $N(m,t)$ mass (density) distribution.

## 3.2 Algorithmic Optimisations

In its raw form without optimisations, the Gillespie algorithm is not particularly fast, because for each aggregation that occurs the recalculation of the event indexing is time consuming. There are a number of ways to optimise the Gillespie algorithm, as reviewed in Mauch and Stalzer [2011]. Broadly speaking, they can be characterised according to whether the number of chemical types remains fairly stable, or whether the number of chemical types increases. For cluster-cluster aggregation, the increase in the number of mass sizes over time is analogous to an expansion of the number of chemical types over time, hence we will concentrate on this strand of algorithm development here. For the other line of development, see its treatment in Mauch and Stalzer [2011] and references therein, and specific developments such as Xiao and Ling [2007] and Slepoy et al. [2008]. The sensitivity of cluster-cluster aggregation to the dynamics of the reaction rate propensities also means that 'tau-leaping' method optimisations (see Gillespie [2007], Mauch and Stalzer [2011] and references therein) are unlikely to be appropriate. (We will not consider optimisations concerned only with parallelisation or GPU (graphics processing unit) utilisation, as these are more concerned with the specifics of implementation.)

In general, when the Gillespie algorithm is running there are two main bottlenecks: The first is the calculation to update the total event rate, and the second is finding which type of reaction or aggregation event is the next one to take place. These processes are related. For chemical systems with a limited number of reaction types it makes sense to have a dependency graph between the reaction types, so that after a reaction has taken place and the associated concentrations of chemical types have changed, only the minimum number of parts of the total reaction rate need to be updated. This dependency graph can be implemented as a sparse matrix. For cluster-cluster aggregation the dependency graph is complete, since any mass size might react with any other (assuming no other restrictions

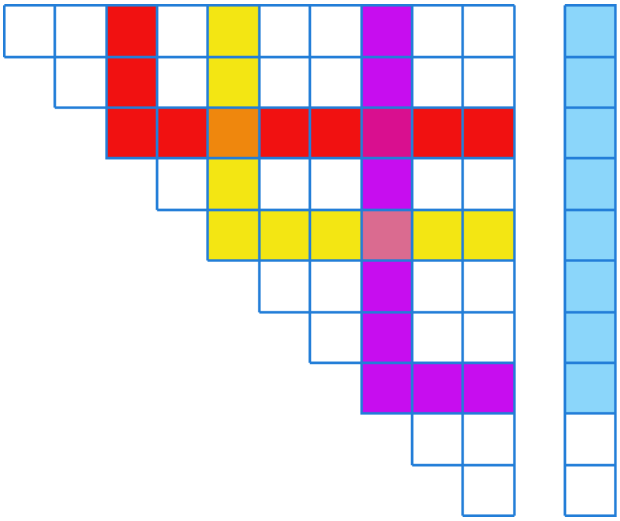

Figure 3.1: A diagram representing the pattern of updates made to the set of event rates after an aggregation between two masses, in this case $3+5 \rightarrow 8$. The large triangular block is the set of aggregation event rates that contribute to the total event rate sum. A brute force algorithm would run along each row in turn, summing the squares in each row as it went. By using row sums instead, updates are limited in effect only to the coloured squares in the triangular block. In reality the update operations are just a small number (2 to 4) of simple arithmetic operations applied only to the row sums to the right of each row, shown here as the column of squares (some blue to depict updates) to the right of the triangular block. Hence total event rate summation is reduced from order $M^2$ to order $M$ operations or fewer. Another array (not shown) of partial sums is readily formed from a running total summing the column of row sums. A binary search capability over the array of partial sums then provides a powerful way to speed up the determination of which type of aggregation event is to take place next (to order $\log(M)$ operations on average).

are in place), and takes the form of a full square matrix. So while various optimisations of the dependency graph are suggested in Gibson and Bruck [2000], Cao et al. [2004], and McCollum et al. [2006], they are not really relevant for cluster-cluster aggregation. Cao et al. [2004], and McCollum et al. [2006] also make use of the dependency graph to sort reaction types in order of likelihood, but again, this is only useful for systems with a restricted set of reaction types. Once the number of reaction types is allowed to expand in potentially unlimited fashion, as in cluster-cluster aggregation, such sorting soon becomes prohibitively expensive.

So the principal optimisation of interest for the Monte Carlo simulation of cluster-cluster aggregation is the storage of partial sums for sections of the total event rate sum. This is then combined with a binary search over the partial sums to obtain the reaction type index, which considerably speeds up the process used in (3.6). For chemical systems this yields an algorithm that runs in $O(\log N_A)$ time [Li and Petzold, 2006].

The use of partial sums also enables minimising the number of updates required for the total event rate sum. There is an increase in the complexity of the code required to achieve this, but (based on prototypes) we anticipate that the resulting algorithm should remain $O(M)$ in the worst case, where $M$ is the maximum mass size in the system. This should permit Monte Carlo simulation of aggregation systems where $M \sim 10^8$ to run in reasonable times. Figure 3.1 depicts how the reduction in the number of update operations is achieved.

## 3.3 Calibration of the Monte Carlo Simulation

### 3.3.1 Scaling Decay Case Distributions

The Monte Carlo simulation of the irreversible aggregation process can be calibrated by checking it against known solutions of the SCE or numerical ODE integrations of a

particular problem. In the sub-gelation regime of the mean-field scaling decay case the analytic solutions for both the time-dependent distribution $N(m,t)$ evolutions and the time-invariant rescaled distributions $\Phi(z)$ of the constant kernel, $K_c = 1$, and the sum kernel, $K_s(m_1,m_2) = (m_1 + m_2)$ are known. Confining discussion to the scaling distributions, the known scaling decay case solutions are, respectively [Leyvraz, 2003]:

$$\Phi_c(z) = 4e^{-2z} \tag{3.10}$$

$$\Phi_s(z) = \frac{1}{\sqrt{2\pi z^3}} e^{-\frac{z}{2}} \tag{3.11}$$

These are normalised distribution functions that presume that the initial mass of the system $\mathscr{M}_1 = 1$. Since, in the absence of gelation phenomena, the total mass of the system remains constant, if the actual initial input, $I_0$, of monomer masses $m_0 = 1$ is some integer amount $I_0 \gg 1$ then in order to match the output from the Monte Carlo simulation and these solutions, it is simply a case of dividing the $N(m,t)$ data by the initial total mass $I_0$ before the rescaling is undertaken.

In order to match the outputs of the Monte Carlo simulation to the known time-dependent analytic solutions for $N(m,t)$ it is also necessary to take into account any scalar prefactor in the kernel function that affects the rate of aggregation. So, for example, if we presume a prefactor of $\frac{1}{4}$ in front of the constant kernel such that our simulation kernel is $K = \frac{1}{4}$, then the rate of aggregation will be slowed by a factor of 4. Hence it should be the case that the Monte Carlo timescale relates to the solution timescale according to $\frac{1}{4}t_{\mathrm{MC}} = t$.

If the behaviour of the Monte Carlo simulation accurately matches the known analytic solutions for both $N(m,t)$ and $\Phi(z)$ outputs, then it can be presumed to be behaving properly. In practice, because the Monte Carlo simulation only approaches the mean-field solutions

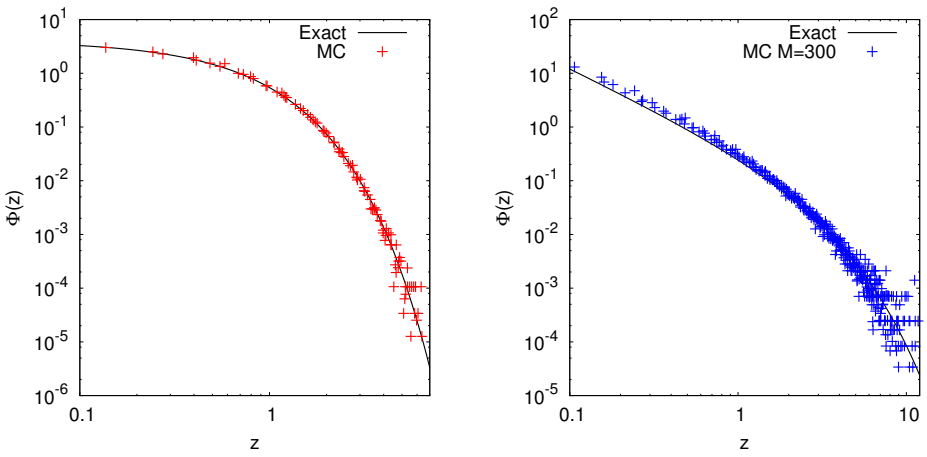


(a) $K = 1$ (b) $K(m_1, m_2) = m_1 + m_2$

Figure 3.2: Calibrations of the Monte Carlo simulation data from single runs with $M = 300$ compared to the exact scaling solutions for (a) the constant $K = 1$ kernel, and (b) the sum kernel. For the sum kernel, the discrepancy at small $z$ arises from finite system size.

in the limit of the Law of Large Numbers, either $I_0$ has to be very large (relative to the maximum mass size of the system), or more practically, a suitable batch of runs with intermediate $I_0$ has to be performed and ensemble averaging of the results undertaken. We found a number of runs $n_r = 20$ to be sufficient for the purposes of our research. However, when finite system size can give rise to discrepancies from the large mass, large times exact scaling solution $\Phi(z)$ (as in Figure 3.2b) comparisons of Monte Carlo data can also be made against finite system size ODE integrations as a further check. We also undertook these checks.

### 3.3.2 Stationary Distributions

For the case of stationary distributions $N(m)$ calibration of the Monte Carlo results is slightly more complicated, though the analytic solutions are known for arbitrary homogeneous kernels [Connaughton et al., 2004]. A stationary distribution arises when there is a constant source of monomer injection at rate $J$ over time, and a maximum upper mass size

$M$ beyond which mass is discarded from the system. The key relationship in this case is that for stable stationary distributions in the local regime, the rate $J$ at which mass enters the system matches the rate at which it leaves. For any given mass size $m$, since $\partial_t mN(m,t) = 0$ in the stationary state, the flux through that mass size is a constant that is independent of $m$ [Connaughton et al., 2008]. Considering only the concentration of monomers $N(m_0) = N_1$ in the discrete case, with $J = 1$ under suitable normalisation, we have the relation:

$$1 = \sum_{m=1}^{M} K(m,1) N_m N_1 \tag{3.12}$$

This represents a rescaled invariant flux relation. If we consider a mass injection at rate $J > 1$, then if the kernel function remains unchanged, there has to be a corresponding proportionate increase in the concentrations according to,

$$J = J \sum_{m=1}^{M} K(m,1) N_m N_1 = \sum_{m=1}^{M} K(m,1) \sqrt{J} N_m \sqrt{J} N_1 \tag{3.13}$$

The relationship between the Monte Carlo simulation's stationary distribution $N_{\mathrm{MC}}(m)$ and the (stable) exact solution $N(m)$ is then given by:

$$N(m) = \frac{N_{\mathrm{MC}}(m)}{\sqrt{J}} \tag{3.14}$$

However, this picture is further complicated if there is any additional prefactor added to the kernel function to control the distribution evolution rates in the Monte Carlo simulation. For example, if we add a prefactor of $1/J$ to the kernel function, then the flux relation has to be adjusted according to:

$$J = \frac{1}{J}J^2 \sum_{m=1}^{M} K(m,1)N_m N_1 = \frac{1}{J}\sum_{m=1}^{M} K(m,1)JN_m JN_1 \tag{3.15}$$

In which case the relationship between the Monte Carlo simulation's stationary distribution $N_{\mathrm{MC}}(m)$ and the corresponding (stable) exact solution $N(m)$ is modified to

$$N(m) = \frac{N_{\mathrm{MC}}(m)}{J} \tag{3.16}$$

Hence the normalisation process has to take into account an interdependence between kernel rates and mass concentrations $N(m)$ in the case of stationary distributions.

This exchange of weighting of factors between the kernel rates and the mass concentrations also has consequences for the evolution of the system. Since the system is initially devoid of mass, and mass is injected at rate $J$, in the absence of any prefactor on the kernel the total mass $\mathscr{M}_1$ on the site is expected (deducing from (3.13)) to grow toward the stationary state according to:

$$\mathscr{M}_1(t) = \sum_{m=1}^{M} m\sqrt{J}N(m,t) \sim Jt \tag{3.17}$$

$$\Rightarrow \frac{d\mathscr{M}_1}{dt} \sim \sqrt{J} \tag{3.18}$$

In order to match up the timescales of the transient growth in both Monte Carlo simulation and an exact ODE integration of the SCE with $J = 1$, it is desirable to map the timescale of the Monte Carlo process so that $d_t\mathscr{M}_1 = 1$. Hence the timescale map becomes $t^* = t_{\mathrm{MC}}\sqrt{J}$.

Again, this process of remapping the timescales is complicated by the introduction of a prefactor on the kernel of the Monte Carlo simulation. For the case given above with a kernel prefactor of $1/J$ the equations for the transient growth become,

$$\mathscr{M}_1(t) = \sum_{m=1}^{M} mJN(m,t) \sim Jt \tag{3.19}$$

$$\Rightarrow \frac{d\mathscr{M}_1}{dt} \sim 1 \tag{3.20}$$

Hence in this case there is no need to remap time to match up the solutions. The results for this case are shown in Figure 3.3.

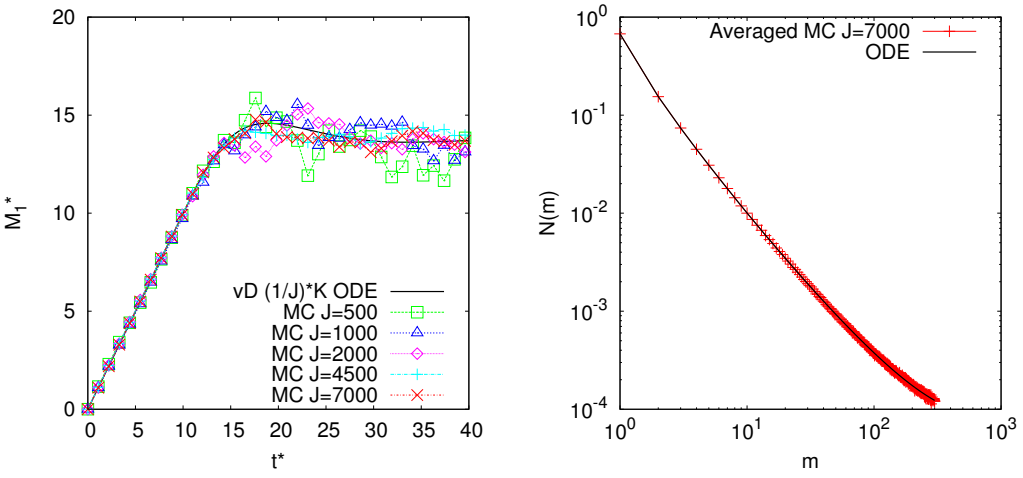


(a) (b)

Figure 3.3: Panel (a) shows rescaling of the MC total site mass evolution to match ODE simulation for the "van Dongen" kernel $K(m_1,m_2) = \frac{1}{J}(m_1^{\mu}m_2^{\nu} + m_2^{\mu}m_1^{\nu})$ with $\mu = -0.25$, $\nu = 0.35$ for a selection of different mass injection rates. The Monte Carlo data shown are for single runs without ensemble averaging. Panel (b) compares a time-averaged stationary state $N(m)$ distribution for the Monte Carlo simulation with the stationary state generated by ODE integration of the SCE. System size was $M = 300$ in all cases.

In similar fashion, if the prefactor on the kernel is $1/\sqrt{J}$ then the adjusting factor for the distribution concentrations $N(m,t)$ and the total mass $\mathscr{M}_1(t)$ is $J^{-\frac{3}{4}}$, and the remapping of time is $t^* = t_{\mathrm{MC}} J^{\frac{1}{4}}$.

Summarising this in general formulae, we have,

$$J = \gamma J^{\beta} \sum_{m=1}^{M} K(1,m) N_m N_1 \qquad \text{with } \gamma = J^{-\alpha} \quad \Rightarrow \beta = \alpha + 1 \tag{3.21}$$

$$N(m)^* = N_{\mathrm{MC}}\, J^{\beta/2} \tag{3.22}$$

$$t^* = t_{\mathrm{MC}}\, J^{1-\beta/2} \tag{3.23}$$

Lastly, for the stationary states, we found it was important to perform ODE integrations of the SCE and match the data against our Monte Carlo simulation data, as once again finite system size could affect the match to the exact analytic solutions by a scalar multiplying factor. In Chapter 5 we also provide a further stationary distribution generation method using a Least Squares method, and this can be used for further checking of the Monte Carlo simulation's behaviour.

## 3.4 Collective Oscillations Around Stationary State Attractors

In the theory of wave kinetics it has been known for some time that only a subset of kernel functions yield stable states with constant flux (in this case, of energy through the wave spectrum) [Zakharov et al., 1992]. In aggregation kinetics, an equivalent notion is that of kernels of the form $K(m_1,m_2) = \frac{1}{2}(m_1^{\mu} m_2^{\nu} + m_2^{\mu} m_1^{\nu})$ that give rise to solutions in the local regime, with $|\nu - \mu| < 1$ [Connaughton et al., 2004]. For systems in the nonlocal regime $|\nu - \mu| > 1$, unstable solutions with significant flux oscillations appear when using exact ODE integration to simulate these systems, with the appearance of an unstable

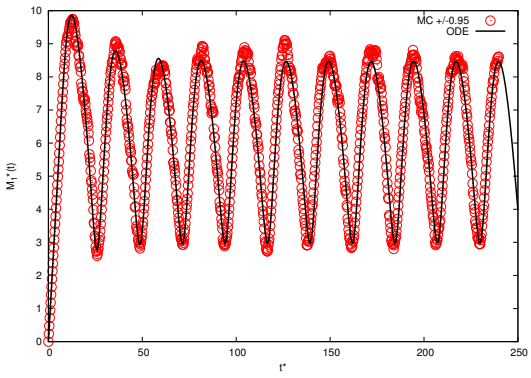


(a)

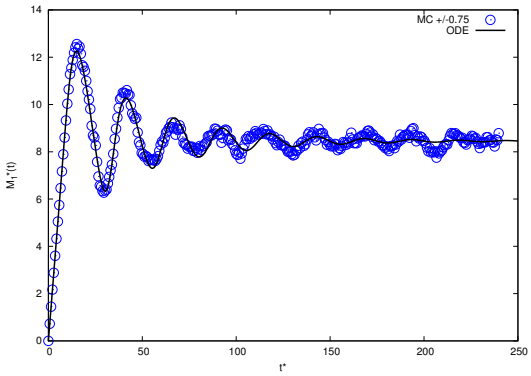


(b)

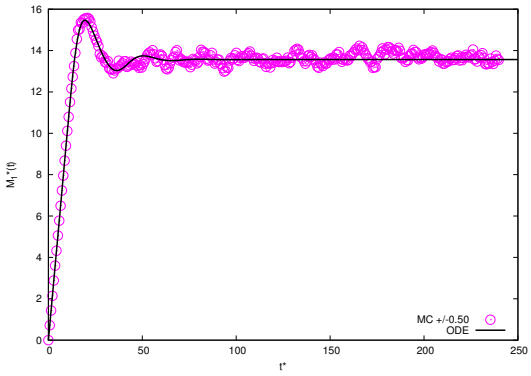


(c)

Figure 3.4: Panel (a) shows driven oscillations of the MC total site mass evolution matching those of ODE simulation for the "van Dongen" kernel $K(m_1,m_2) = \gamma\frac{1}{2}(m_1^\mu m_2^\nu + m_2^\mu m_1^\nu)$ with $\mu = 0.95$, $\nu = -0.95$, with $J = 2000$ and $\gamma = \frac{1}{50000}$. Panel (b) is for $\mu = 0.75$, $\nu = -0.75$, and panel (c) is for $\mu = 0.50$, $\nu = -0.50$. The Monte Carlo data shown are for single runs without ensemble averaging. System size was $M = 300$ in all cases.

state depending upon the upper cutoff mass size $M$. It was assumed that in real aggregation systems, noise would typically disrupt concerted oscillations, allowing the system to eventually approximate a stable state. So a thorough study of collective oscillations in aggregation systems had not previously been undertaken.

During the course of the research for this thesis Monte Carlo simulations of finite systems in the nonlocal regime, with kernel parameterisations that were known to yield unstable distributions with sizeable flux oscillations under exact ODE integration, were tested. Despite the presence of significant noise throughout the system evolution, the Monte Carlo simulations also exhibited sustained bulk flux oscillations. Examples are shown in Figure 3.4 for a system of size $M = 300$ where the different effects obtained when the kernel is far away from the local regime (Figure 3.4a), on the border of the local regime (Figure 3.4c), and at parameterisation in between (Figure 3.4b), can be seen. As a result of determining that the oscillations remained in the presence of noise, further research on the topic of collective oscillations (in the absence of noise) was then pursued in Ball et al. [2012].

In Ball et al. [2012] we investigated how the mass flux is carried from source to sink in the nonlocal regime. It was found that for a range of values of $M$ the numerical solution retained persistent oscillations in the total mass on the site. This occurs even if the simulation is started from an exact stationary state and perturbed slightly. Analysis confirmed the presence of a linear instability in the system, with the stationary state undergoing a Hopf bifurcation to produce a limit cycle as $M$ is increased.

The intuitive explanation of the mechanism that creates the oscillations is that the nonlocality implies that larger masses aggregate with the smaller masses very efficiently. When this occurs, the larger masses leave the system very rapidly, at the same time as the smaller masses are depleted, and the total mass in the system drops significantly. There is then

a delay before more of the larger masses are created, during which the remaining masses in the spectrum aggregate more slowly. The smaller masses and the larger masses then gradually replenish, with the creation of larger masses accelerating as more of the smallest masses are injected into the system. The larger and smaller masses subsequently aggregate strongly with each other, and cause another pulse of mass to exit the system rapidly.

From this explanation, it would be expected that the typical mass of the system, $s(t)$ would oscillate with a frequency matching that of the overall oscillations in the total mass of the system. For the range of maximum masses $M$ where oscillations occur, we might also expect the amplitude of oscillations to grow as $M$ is increased. From numerical investigations it was also seen that the rapid exit of larger masses almost reset the total mass in the system to zero. In addition, it appeared that the mass in each pulse grew linearly in time up to a maximum. However, the average mass flux through a particular mass size remained constant.

From the above facts it was possible to deduce (see Ball et al. [2012]) that the typical mass grows according to,

$$s(t) \sim t^{2/(1-\nu-\mu)} \tag{3.24}$$

Then estimating the period of oscillation $\tau_M$ as the time required for the typical mass to reach $M$ yields:

$$\tau_M \sim M^{(1-\nu-\mu)/2} \tag{3.25}$$

Assuming the linear growth of mass pulses in time according to $Jt$ then provides the amplitude of the oscillations $A_M$ as:

$$A_M \sim JM^{(1-\nu-\mu)/2} \tag{3.26}$$

Applying these equations to the data from (ODE) numerical simulations confirmed their validity, providing evidence of the scaling of the oscillations in the total mass as $M$ was increased, for a fixed value of $|\nu - \mu|$ [Ball et al., 2012]. For a fixed value of $M$ further increase of $\nu$ restores stability to the system for reasons that are not yet clear.

We remark that the kernel prefactor $\gamma$ can be used to tune the Monte Carlo simulation, controlling the aggregation rates of the system so that particular features can be better observed. However, as was shown above in the discussion of the calibration of the Monte Carlo system, the kernel prefactor has an effect on the total amount of mass found in the system. The smaller $\gamma$ is, the more the aggregation rate is slowed, and (for some injection $J$) the more mass will pile up on the site. The net effect is then that a smaller $\gamma$ reduces the amount of noise in the system, as the movement of single masses have proportionately less effect on the total mass. The simulation then better approximates an ODE integration. An ability to control the amount of noise in an evolution will be important for further studies of collective oscillations with noise and the phenomenon of quasicycles in aggregation reported in the next section.

## 3.5 Noise-Driven Quasicycles Around Stationary State Attractors

For a system of finite mass spectrum containing a number of masses below a value that would allow the Law of Large Numbers to reproduce ensemble averaging toward the mean-field limit, the Monte Carlo process matches the Marcus-Lushnikov process (see Aldous [1999], Fournier and Giet [2004]). This makes Monte Carlo simulation an ideal tool for investigating cluster-cluster aggregation phenomena in which noise plays a non-trivial role. One such phenonemon is the capacity of intrinsic noise, caused by fluctuations in population levels in a dynamical system, to generate and sustain noise-driven cycles (also called stochastic cycles or quasicycles). These have been observed and discussed for some time in connection with low-dimensional predator-prey-type models [Bartlett, 1957] [Nisbet and Gurney, 1976] [Nisbet and Gurney, 1982] [Renshaw, 1991] [Gurney and Nisbet, 1998] [Mallick and Marcq, 2003] [Morita et al., 2005] [McKane and Newman, 2005] [Mobilia et al., 2007]. Recently, mathematical techniques for the analysis of quasicycles have reached maturity [Boland et al., 2008, 2009] (see also Shuda et al. [2009] and Tomé and de Oliveira [2009]) by exploiting an inverse system size expansion developed by van Kampen [2007].

Given the properties of collective oscillations investigated in Ball et al. [2012] it is perhaps not surprising that certain nonlocal parameterisations of aggregation systems of particular sizes should exhibit quasicycles in Monte Carlo simulation. In the following, we present preliminary evidence that indicates that this is indeed the case.

Using the methods in Ball et al. [2012] and some experimentation, we can construct an ODE integration that represents a sensitive yet damped system, prone to oscillations of the mass flux for some time after the initial transient build up of mass on the site. Ultimately

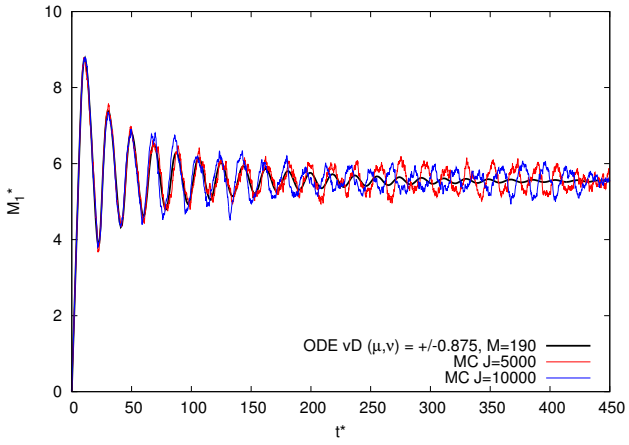


(a)

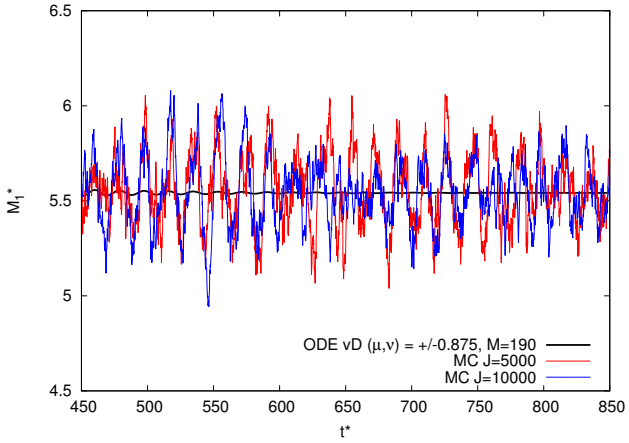


(b)

Figure 3.5: Comparisons of an ODE integration with Monte Carlo simulations with $M = 190$ for the "van Dongen" kernel $K_{\mathrm{MC}}(m_1, m_2) = \gamma \frac{1}{2}(m_1^{\mu} m_2^{\nu} + m_2^{\mu} m_1^{\nu})$ with $\mu = 0.875$, $\nu = -0.875$, with $J_{\mathrm{MC}} \in \{5000, 10000\}$ and $\gamma = \frac{1}{25000}$. Panel (a) shows times $0 < t \leq 450$; panel (b) zooms in on the interval $450 < t \leq 850$. The Monte Carlo data shown are for single runs without ensemble averaging.

though, the damping wins and the system will settle to a stable stationary distribution. By feeding the same parameters into a Monte Carlo simulation of the aggregation system, and controlling the amount of noise, it is possible to test whether the presence of noise will cause the system to maintain an unstable oscillatory state.

In Figure 3.5, we show the results for a system with upper cutoff mass $M = 190$ using the kernel $K(m_1, m_2) = \frac{1}{2}(m_1^\mu m_2^\nu + m_2^\mu m_1^\nu)$ with $\mu = 0.875$, $\nu = -0.875$. The system was run for a period $0 < t < 860$. In Figure 3.5b it can be seen that the oscillations of the ODE integration die away to zero, while the oscillations of correponding Monte Carlo simulations with noisy evolution appear to be sustained. Most of the variance in the Monte Carlo time series is caused by the noise (via the mechanism of stochastic amplification), so the real question is whether the time series also contains evidence of a sustained sinusoidal signal.

The theory in Ball et al. [2012] suggests that for systems of size $M = 190$ but lesser nonlocality, the damping effect should be stronger, and in the presence of noise long time correlations in the total mass $\mathscr{M}_1(t)$ on the site should be lost. In Figure 3.6a we compare the (sample) autocorrelation functions (ACFs) of $\mathscr{M}_1(t)$ for the three kernels with $(\mu, \nu) \in \{\pm 0.875, \pm 0.75, \pm 0.52\}$. Only the $(\mu, \nu) = \pm 0.875$ case exhibits sinusoidal correlations over large lag times $\tau$. In the other two cases noise acts disruptively.

Moreover, by comparing the ACFs of the Monte Carlo and ODE integrations for the $(\mu, \nu) = \pm 0.875$ case, we see in Figure 3.6b that at large lag times $\tau$ the ACF of the Monte Carlo integration has a fixed amplitude and frequency, while that of the ODE integration continues to decay. This suggests that noise is having a driving effect sustaining the underlying sinusoidal signal in the time series in the manner of a phase-remembering quasicycle [Nisbet and Gurney, 1982] [Renshaw, 1991].

It is suggested in Boland et al. [2008, 2009] that generalisations of the mathematical methods therein could be deployed against high dimensional systems. (C.f. van Dongen [1987b] where fluctuations of $N(m,t)$ in decay case evolutions are studied using the inverse system size expansion.) However, the specifics of adapting the analysis to stationary state aggregation evolutions with noise need to be undertaken to confirm this. Longer time series

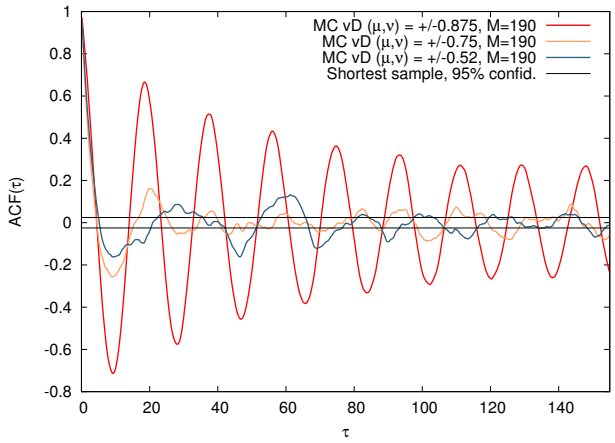


(a)

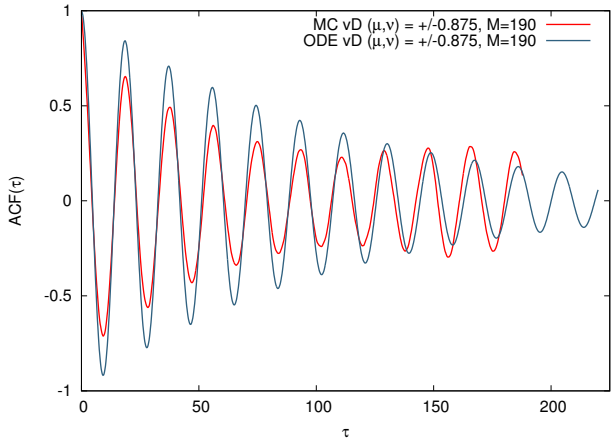


(b)

Figure 3.6: Panel (a) shows the autocorrelation function (ACF) for the total mass $\mathscr{M}_1(t)$ of Monte Carlo simulations with $M = 190$ for the stationary case SCE with the "van Dongen" kernel $K_{\mathrm{MC}}(m_1, m_2) = \gamma\frac{1}{2}(m_1^{\mu} m_2^{\nu} + m_2^{\mu} m_1^{\nu})$ with $(\mu, \nu) \in \{\pm 0.875, \pm 0.75, \pm 0.52\}$, $J_{\mathrm{MC}} = 5000$ and $\gamma = \frac{1}{25000}$. Only the $(\mu, \nu) = \pm 0.875$ case exhibits sinusoidal correlations over large lag times $\tau$. Panel (b) compares the ACFs for $\mathscr{M}_1(t)$ of Monte Carlo and ODE simulations, with $(\mu, \nu) = \pm 0.875$, showing that at large $\tau$ the correlation amplitudes are sustained in the Monte Carlo case, suggesting driving. The Monte Carlo data shown are for single runs without ensemble averaging.

from Monte Carlo simulations of aggregation systems will be needed to improve the evidence for investigation of the full properties of the effect. A tantalising possibility is that the domain of nonlocal parameterisations for certain sizes of aggregation systems will pro-

vide a spectrum to investigate the transition from phase-forgetting to phase-remembering quasicycles in continuous fashion.

# Chapter 4

# Revisiting the Wright-Ramkrishna Inverse Method

The purpose of the work in this chapter is to revisit the inverse method in Wright and Ramkrishna [1992], partly to familiarise ourselves with the technical difficulties involved in inverting from scaled mass distribution data to obtain estimated kernels, and partly to assess whether the method is capable of producing accurate inversions for a simple class of kernels with fractional exponents. The latter is an important property of a desirable method because many problems concerned with the aggregation or coagulation of masses might be expected to have fractional exponents within the aggregation rate function. Examples are problems where particles diffuse with random walk motions, or those that involve particle motion within a turbulent medium where the energy or momentum transfers could be expected to exhibit (derived) fractional exponents that impact upon the aggregation rates.

A portion of the following work has been published in our paper Connaughton and Jones [2011]. Here we add to that some additional treatment of a few subtleties of the Wright and Ramkrishna [1992] method and some further assessments of its capabilities.

The Wright and Ramkrishna [1992] paper consists of two main parts (besides the introduction). The first part contains a valuable analysis of the theory surrounding the scaled Smoluchowski equation, oriented towards the problem of inversion. The second part constructs an inverse method based upon the results of this analysis. We stress here that the input data to the method is a *scaled* mass distribution for a decay case problem. More on this below.

## 4.1 The Wright-Ramkrishna Inverse Method

### 4.1.1 Derivations and Consistency

Following the text of Wright and Ramkrishna [1992], the Smoluchowski Coalescence Equation [Smoluchowski, 1917] is initially recast in terms of the cumulative density fraction,

$$F(m,t) = \int_0^m \tilde{m} N(\tilde{m},t)\, d\tilde{m} \tag{4.1}$$

We provide a version of this initial derivation in Appendix A as an aid. The starting point for the development of the inverse method is then the equation,

$$\frac{\partial F(m,t)}{\partial t} = -\int_0^m \int_{m-\tilde{m}}^{\infty} K(\tilde{m},m_1) \frac{dF(m_1,t)}{m_1} dF(\tilde{m},t) \tag{4.2}$$

This equation (4.2) needs to be transformed into a scaling form. As mentioned earlier in Chapter 2, the scaling hypothesis holds if the mass distribution obeys the similarity transformation,

$$N(m,t) = s(t)^a \Phi(z) \tag{4.3}$$

Where $z = m/s(t)$, $s(t)$ is a function which tracks the typical mass size of the $N(m,t)$ distribution over time, and $\Phi(z)$ is the (time-invariant) scaling mass density distribution. For a non-gelling system, the total mass is conserved. Assuming a suitable normalisation the total mass in the system can be considered to be equal to one, and we have, for all times $t \geq 0$:

$$F(\infty,t) = \int_0^\infty \tilde{m} N(\tilde{m},t)\, d\tilde{m} = 1 \tag{4.4}$$

Here $F(\infty,t)$ is equal to the first moment, $\mathscr{M}_1$ of the distribution $N(m,t)$, so mass conservation implies $\mathscr{M}_1 = 1$ for all times $t \geq 0$. Substituting the similarity transformation into the integrand of the moment $\mathscr{M}_1$ gives,

$$\int_0^\infty z s(t)\, s(t)^a \Phi(z)\, s(t) dz = \int_0^\infty s(t)^2 s(t)^a z \Phi(z)\, dz = 1 \tag{4.5}$$

Consistency with mass conservation for the rescaled mass distribution $\Phi(z)$ requires that $a = -2$. In the Wright and Ramkrishna [1992] paper an alternative form of the similarity transformation is used. First, differentiation of the cumulative mass fraction with respect to mass yields,

$$N(m,t) = \frac{1}{m} \frac{\partial F(m,t)}{\partial m} \tag{4.6}$$

Then a direct mapping to a scaling (mass fraction) distribution form is asserted as $F(m,t) \rightarrow f(z)$. It then follows that,

$$N(m,t) = \frac{1}{zs(t)} \frac{df(z)}{dzs(t)} = s(t)^{-2} \frac{f'(z)}{z} \qquad \text{and,} \tag{4.7}$$

$$\frac{f'(z)}{z} = \Phi(z) \tag{4.8}$$

Applying the same $F(m,t) \rightarrow f(z)$ mapping to (4.2), and using the fact that $\frac{df(z)}{dz} = f'(z)$ we get,

$$\frac{df}{dz}\frac{dz}{dt} = -\iint_{-\infty}^{\infty} [0 \leq xs(t) \leq zs(t)][(z-x)s(t) \leq ys(t) \leq \infty] K(xs(t), ys(t)) \frac{df(y)}{ys(t)} df(x) \tag{4.9}$$

$$-zf'(z)\frac{1}{s(t)}\frac{ds}{dt} = -\frac{1}{s(t)} \iint_{-\infty}^{\infty} [0 \leq x \leq z][(z-x) \leq y \leq \infty] K(xs(t), ys(t)) f'(x) \frac{f'(y)}{y} dydx \tag{4.10}$$

$$zf'(z) = \frac{1}{s'(t)} \int_0^z f'(x) \int_{z-x}^{\infty} \frac{f'(y)}{y} K(xs(t), ys(t)) dydx \tag{4.11}$$

Using the instructions in Wright and Ramkrishna [1992] we then make use of the homogeneity of the kernel and the rate of evolution of the typical mass $s(t)$,

$$K(xs(t), ys(t)) = s(t)^{\lambda} K(x,y) = s(t)^{\lambda} K(y,x) \qquad \text{WR92.(17)} \tag{4.12}$$

$$\frac{ds(t)}{dt} = Ws(t)^{\lambda} \qquad \text{WR92.(18)} \tag{4.13}$$

Here, $W$ is known as the separation constant, a constant of proportion in the relationship between the rate of change of the typical mass and the homogeneity of the kernel whose

value depends on how $s(t)$ is defined (see [van Dongen and Ernst, 1988, §1][Leyvraz, 2003, §3.1][Krapivsky et al., 2010, §5.4]). Making the appropriate substitutions into (4.11) yields Eqn. 69 of Wright and Ramkrishna [1992], which is the essential equation underlying the construction of the inverse method.

$$zf'(z) = \int_0^z f'(x) \int_{z-x}^{\infty} \frac{f'(y)}{y} \frac{K(x,y)}{W} dydx \tag{4.14}$$

We remark here that in Leyvraz [2003] the time-dependent mass distribution is defined as $N(m,t) = Ws(t)^{-2}\Psi(z)$ which has the consequence that $W$ can be cancelled from the equivalent version of (4.14) if $\Psi(z)$ is taken to be the scaling distribution. This does not alter the fact that in order to recover the kernel function at some point $W$ has to be determined. If there are enough time snapshots of $N(m,t)$ then $s(t)$ can be recovered from the knowledge [Wright and Ramkrishna, 1992][Leyvraz, 2003] that,

$$s(t) = \frac{\mathscr{M}_2(t)}{\mathscr{M}_1(t)} \tag{4.15}$$

$$\text{where } \mathscr{M}_p = \int_0^{\infty} \tilde{m}^p N(\tilde{m},t)\, d\tilde{m} \tag{4.16}$$

Since (4.13) is a deterministic ODE, if the initial condition $s(0)$ is known as well as $s(t)$ for the range of times $t$ under consideration, then $W$ and $\lambda$ are uniquely determined by their relationship in (4.13). Solving (4.13) for $s(t)$ provides the equation,

$$s(t) = \left[(1-\lambda)Wt + s(0)^{1-\lambda}\right]^{\frac{1}{1-\lambda}} \tag{4.17}$$

Fitting the RHS of this expression to the data provided by using (4.15) could then, in principle, give estimates for $W$ and $\lambda$. Hence, in order to recover $K(x,y)$ the method in Wright and Ramkrishna [1992] actually requires two parameter estimation processes to be undertaken (see also Wright et al. [1992]).

It is asserted in Leyvraz [2003] that for decay case aggregation systems in the scaling limit, $m \to \infty, t \to \infty$ with $m/s(t)$ fixed, given a suitable definition of convergence to a scaling distribution, that for a homogeneous kernel all 'reasonable' initial conditions will result in a scaling distribution in that limit. So in that limit, all such initial conditions can be considered to be equivalent to $s(0) = 1$. This initial condition would provide formal uniqueness for the pair $(W, \lambda)$ when fitting data using (4.17). Unfortunately, real data for finite mass systems only approximately conforms to the scaling hypothesis, so presumptions cannot be made about unknown initial conditions.

An alternative approach, taken in Connaughton and Jones [2011], which avoids having to obtain an explicit value for $W$ is to tacitly assume a rescaled time $\tau = Wt$ so that $\tilde{z} = m/s(\tau)$. It can then be consistently asserted that,

$$\frac{ds(\tau)}{d\tau} = s(\tau)^{\lambda} \tag{4.18}$$

$$N(m,\tau) = s(\tau)^{-2}\frac{g(\tilde{z})}{\tilde{z}} \tag{4.19}$$

Applying this rescaling throughout the derivation above provides,

$$\tilde{z}g'(\tilde{z}) = \int_0^{\tilde{z}} g'(\tilde{x}) \int_{\tilde{z}-\tilde{x}}^{\infty} \frac{g'(\tilde{y})}{\tilde{y}} K(\tilde{x},\tilde{y}) d\tilde{y} d\tilde{x} \tag{4.20}$$

As long as the original $f'(z)/z$ calculated using $s(t)$ is the same as the $g'(\tilde{z})/\tilde{z}$ that would be calculated using $s(\tau)$, then this approach is valid. Tests on decay case $N(m,t)$ distributions generated using sum kernels when $s(0) = 1$ indicate that as long as the resulting $N(m,t)$ data is normalised so that $\mathscr{M}_1 = 1$, then subsequently rescaling using an $s(t)$ generated from (4.15) will yield a $g'(\tilde{z})/\tilde{z}$ such that $W = 1$ can be assumed. If $W = 1$, then $f'(z)/z = g'(\tilde{z})/\tilde{z}$. Normalisation of the $N(m,t)$ data also implies that in principle the initial mass of the system does not need to be known. In this case, $K(\tilde{x},\tilde{y})$ is directly representative of the rescaled kernel function.

However, we stress that (as is shown in more detail in Chapter 5) tests revealed that this approach only holds for certain forms of kernel function, of which the sum kernels are a subset. For other kernel forms $W \neq 1$ is possible, and adequate estimation of $W$ then depends heavily on successful retrieval of $\lambda$ from the main inverse method. As will be seen later in §4.2 the results from the method in Wright and Ramkrishna [1992] do not permit ready inference of $\lambda$ from the data.

### 4.1.2 Numerical Approximation

Returning to the development of the main inverse method, because the term on the right-hand side of (4.14) is linear in respect of the kernel function, it can considered as an operator equation of the form,

$$\mathbf{b} = \mathbf{A}\mathbf{k} \tag{4.21}$$

As noted in [Wright and Ramkrishna, 1992, § 5.1] equation (4.14) is a "Volterra-type integral equation of the first kind" which can be ill-posed, with small perturbations in the LHS giving rise to large deviations from the optimal result for the retrieved kernel on the

RHS. This problem can be combatted, to some degree, by deploying classic Tikhonov regularisation (see e.g. [Aster et al., 2005, Ch. 5]), so that the inverse problem is then concerned with the minimisation of,

$$\min_{\mathbf{k}} \|\mathbf{A}\mathbf{k} - \mathbf{b}\|_p^2 + \rho_{\text{reg}} \|\mathbf{k}\|_q^2 \tag{4.22}$$

Where the subscripts $p$ and $q$ represent the possibility that two different norms are applied, and $\rho_{\text{reg}} \|\mathbf{k}\|_q^2$ is the regularisation term with $\rho_{\text{reg}}$ a scalar tuning parameter.

However, in practice, assuming a suitable discretisation of the data in the observed mass distribution, $\mathbf{b}_N = \{b_i\}$, $i = 1, \ldots, N$, we still have an inverse problem with $N$ equations and $N^2$ unknowns in the kernel $K(x,y)$. So the inverse problem in this form is hugely under-determined and hence remains ill-posed (owing to the enormous potential for non-uniqueness of possible solutions). Therefore, in order to render the inverse problem more feasible techniques also need to be employed to reduce the number of parameters that have to be estimated. In Wright and Ramkrishna [1992] this problem is solved (to a degree) by representing the kernel using a basis of orthogonal functions, in this case Laguerre polynomials. The choice of Laguerre polynomials, as compared with any other orthogonal polynomial basis, is partly because their domain is $(0, \infty)$ and the kernel is $K : \mathbb{R}^+ \times \mathbb{R}^+ \to \mathbb{R}^+$. But, as is documented in Wright and Ramkrishna [1992], there is also a useful relationship between their inner product and (4.14) which permits the kernel function to be written as a linear combination of appropriate basis function products $l_n(x,y)$ weighted by scalar coefficients $a_n$ such that:

$$\frac{K(x,y)}{W} = \sum_n a_n l_n(x,y) \tag{4.23}$$

$$\text{where } l_n(x,y) = L_i(x)L_j(y) \tag{4.24}$$

With $n = (i-1)n_{\text{basis}} + j$ being an indexing scheme that combines the separate $i$ and $j$ polynomial indexes on the $x$ and $y$ dimensions, respectively, into a single index $n$; and $n_{\text{basis}}$ is the number of basis (Laguerre polynomial) functions in each dimension. That is, if $n_{\text{basis}} = 4$ then $i,\ j = 1,\ldots,4$ and (without elimination of symmetries) there will be 16 $L_i(x)L_j(y)$ combinations of basis pairs. So $n$ will run from 1 to 16. (This numerical indexing scheme should not be confused with the fact that the first Laguerre polynomial is often given the notation $L_0(x)$ in texts.)

Given this linear sum representation of the kernel function, the inverse problem can be suitably discretised in terms of an operator matrix $\mathbf{X}$ with entries defined as:

$$X_{st} = \int_0^{z_s} dx f'(x) \int_{z_s - x}^{\infty} dy \frac{f'(y)}{y} l_t(x,y) \tag{4.25}$$

The operator matrix $X_{st}$ acts on the coefficients $\mathbf{a} = (a_i)_{i=1}^n$, such that the numerical minimisation is described by:

$$\min_{\mathbf{a}} \|\mathbf{X}\mathbf{a} - \mathbf{b_N}\|_2^2 + \rho_{\text{reg}} w(\mathbf{a}) \tag{4.26}$$

Where $w(\mathbf{a})$ is some suitable function that makes the regularisation process work effectively. As with equation (4.22) above, $w(\mathbf{a}) = \|\mathbf{a}\|_2^2$ is the option for classic zero-th order

Tikhonov regularisation.

### 4.1.3 Regularisation Issues

The norm notation has been dropped from the regularisation function in (4.26), because our experiments yielded that the traditional $l_2$-norm did not work well. Through further experimentation we found an effective $w$ function of the form:

$$w(\mathbf{a}) = \sum_i \log(|a_i| + 1) = \log\left[\prod_i (|a_i| + 1)_i\right] \tag{4.27}$$

It is not clear (see commentary below) why this function should be superior to many others of similar geometry. It was chosen to sustain the effect of regularisation when some of the $a_i$ are very small. A possibility is that it has a fractional exponent polynomial behaviour when the regularisation parameter is applied and that this is somehow useful in minimisations with kernel homogeneity $0 < \lambda < 1$. A basic rearrangement of the regularisation function exposes the polynomial form.

$$\rho_{\text{reg}} w(\mathbf{a}) = \log\left(\left[\prod_i (|a_i| + 1)_i\right]^{\rho_{\text{reg}}}\right) \tag{4.28}$$

The value of this modified regularisation method is questionable for reasons outlined below. For any regularisation function there are many methods for attempting to select an optimal value of the regularisation parameter $\rho_{\text{reg}}$, but none of these methods is perfect (see Doicu et al. [2010], Bauer and Lukas [2011]). Analytical justifications for these methods also do not always transfer to practical situations [Bauer and Lukas, 2011]. Methods for choosing $\rho_{\text{reg}}$ on *a priori* grounds are typically ruled out as being impractical because sufficient prior knowledge of solutions' properties generally does not exist for real experimental

observations [Bauer and Lukas, 2011].

One of the simplest methods for estimating the optimal regularisation parameter value is the L-Curve method given in Hansen [2001] which plots the norm of the residual against the norm of the solution for different values of $\rho_{\text{reg}}$. In nice cases this results in a curve with a clear L shape, with the optimal regularisation parameter value being found near the corner of the L. However, an assumption in Hansen [2001] is that the points for the regularisation parameter appear in order on the L-Curve, and that hence it is trivial to choose the regularisation parameter value as being a point near the corner.

As is noted in Connaughton and Jones [2011], the $l_2$-norm did allow the attempted use of the L-Curve method [Hansen, 2001],[Doicu et al., 2010] to attempt to estimate the optimal value of $\rho_{\text{reg}}$, but the overall results of the inversions were poor in key cases. Switching to the custom function $w(\mathbf{a})$ produced results which qualitatively appeared superior, but unfortunately it also prevented the construction of plausible L-Curves, for reasons that are also not clear.

In addition, for our modification of the Wright and Ramkrishna [1992] method, plotting 3-D curves with the regularisation parameters ordered on a third axis revealed that the assumption about the ordering of points along the L-Curve generated by successive values of $\rho_{\text{reg}}$ can often be false, misleading the choices of regularisation parameter value if care is not taken. While it is possible that our problem is too smooth (matching the limitations of the L-Curve method noted in Hansen [2001]) it is also possible that some other property could be the cause. Naive use of the L-Curve method is therefore ruled out.

Furthermore, there is a sense in which we can rule out any of the *a posteriori* and the data-driven methods reviewed in [Bauer and Lukas, 2011] since both inversions from exact scaling distribution data and Monte Carlo simulation data (whose noisy distributions can be

turned into almost exact data through ensemble averaging) yielded that a major weakness for the Wright and Ramkrishna [1992] inverse method is in the accuracy with which $\Phi(z)$ is estimated by fitting with a sum of Gamma distributions, prior to inversion. Stronger evidence for the sensitivity of this inverse problem to this issue is provided in Chapter 5. Our data is therefore not noisy in the sense which would make these regularisation parameter choice methods useful.

It is also shown below in § 4.3 that there is an additional inability of the Wright and Ramkrishna [1992] method to represent a class of kernels with fractional exponents with a high degree of accuracy. Therefore, we are *actually* attempting to find a means of regularisation (and its associated regularisation parameter) that somehow compensates for (in some cases) both systematically inaccurate data inputs and a systematic inability to represent the solution properly. So, with the benefit of hindsight, the fact that our modified regularisation function somehow conjures up solutions that look plausible probably should not be considered at all reassuring. The results shown below in § 4.2, especially in the cases of the kernels with fractional exponents, should therefore be treated as potentially misleading.

## 4.2 Inversion Results

The method was implemented in *Mathematica*$^{\text{TM}}$ v.7, following Wright and Ramkrishna [1992] as closely as possible. For application of the method to the exact $\Phi(z)$ data, minimisations were conducted with 30 values of $\rho_{\text{reg}}$ chosen logarithmically spaced in the interval $I_E = [1 \times 10^{-10}, 1.0]$. Since the results of the application of this method to exact data were favourable, a Monte Carlo (MC) method (outlined in Chapter 3 and implemented by the author) was used to generate noisier data for the sum kernels,

$$K(x,y) = \frac{1}{2}(x^\lambda + y^\lambda) \tag{4.29}$$

With $\lambda \in \{0.0, 0.25, 0.50, 0.75, 1.0\}$. The raw MC data contained noise, partly because of its simulation of zero-dimensional Marcus-Lushnikov [Aldous, 1999][Fournier and Giet, 2004] aggregation dynamics for a finite system (with maximum mass size $M = 300$) and partly because at larger values of $m$ masses larger than the finite system maximum mass size cutoff were discarded. Minimisations using the raw MC data were also conducted using 30 values of $\rho_{\text{reg}}$ chosen as stated earlier.

### 4.2.1 Sum Kernel: Monte Carlo Data

Since the results for the exact data and the Monte Carlo data were comparable, we discuss only minimisations against the latter dataset here. In Figure 4.1 we show the inversions results for $\lambda \in \{0.0, 1.0\}$ when deployed on the Monte Carlo simulated data. In this figure, and later ones, for each kernel we show the edge $K(0,y)$ and the diagonal $K(y,y)$. Our results differ somewhat from those shown in Wright and Ramkrishna [1992], and checks indicated that we can only attribute this difference to the contemporary minimisation methods used. We also remark that in the $\lambda = 0.0$ case there was a tendency for the method to generate constant solutions very close to the desired solution when the regularisation was approaching $\rho_{\text{reg}} = 1.0$. There is some concern that in this particular case some of these constant solutions might actually be artifacts of the method 'stalling' when the regularisation is too dominant, as similar constant functions appear in two of the cases where the kernel has fractional homogeneity, as seen in Figure 4.2. Nevertheless, the inverse method is seen to return plausible results in all cases before the onset of such stalling.

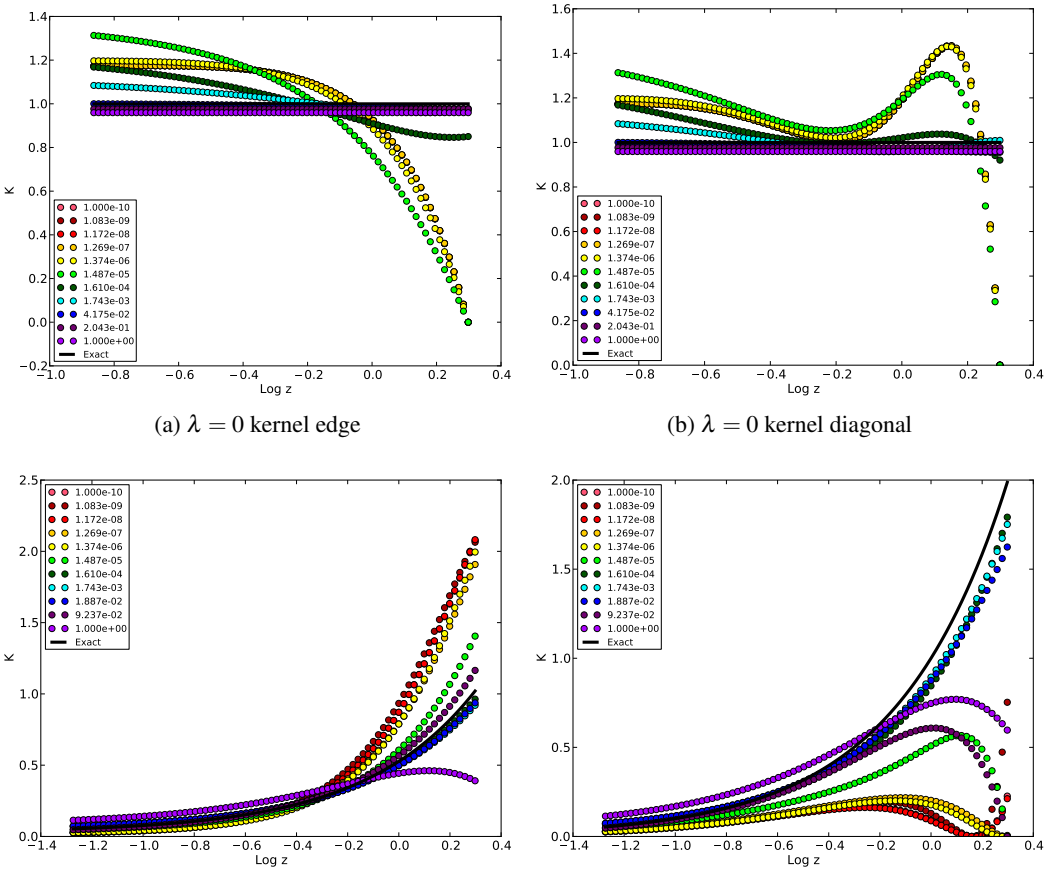


(a) $\lambda = 0$ kernel edge

(b) $\lambda = 0$ kernel diagonal

(c) $\lambda = 1.00$ kernel edge

(d) $\lambda = 1.00$ kernel diagonal

Figure 4.1: Inversions from Monte Carlo data, $\lambda \in \{0.0, 1.0\}$

The results for the sum kernels with fractional homogeneity exponents are shown in Figure 4.2. It can be seen that for the cases $\lambda \in \{0.5, 0.75\}$ that plausible results were obtained for values of the regularisation parameter in a range approximately $10^{-3} \lesssim \rho_{\text{reg}} \lesssim 10^{-2}$. However, in the $\lambda = 0.25$ case it can be seen that the results overall are less plausible than in the other cases. We investigate whether this is likely to be a consequence of the limits of representation using Laguerre polynomial basis functions in the next section.

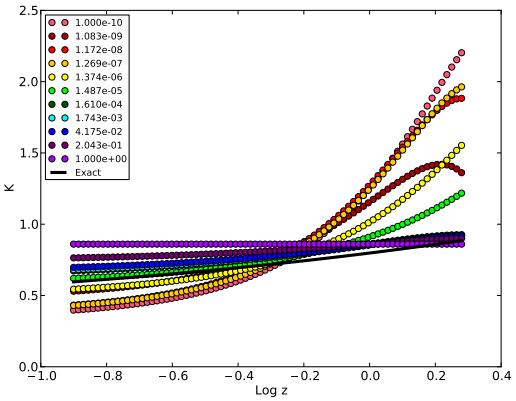


(a) $\lambda = 0.25$ kernel edge

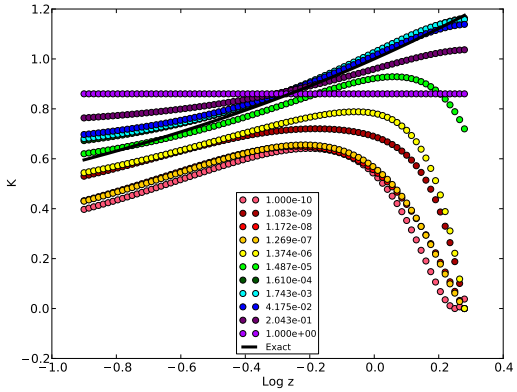


(b) $\lambda = 0.25$ kernel diagonal

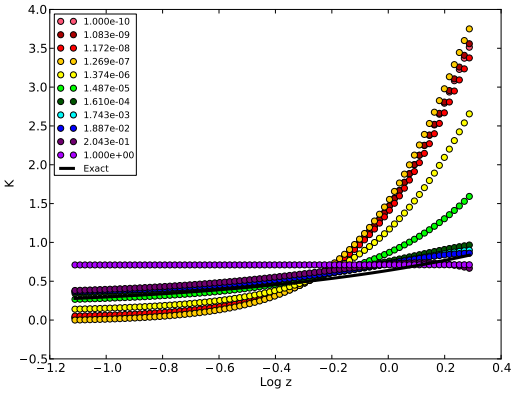


(c) $\lambda = 0.50$ kernel edge

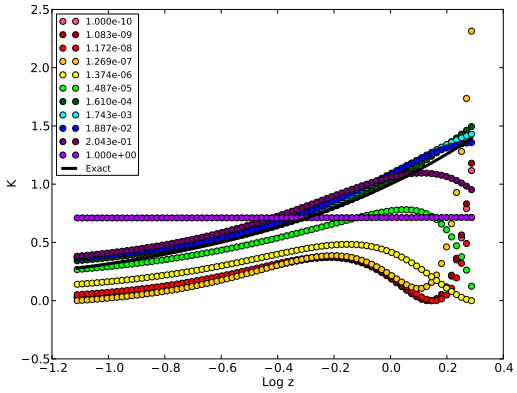


(d) $\lambda = 0.50$ kernel diagonal

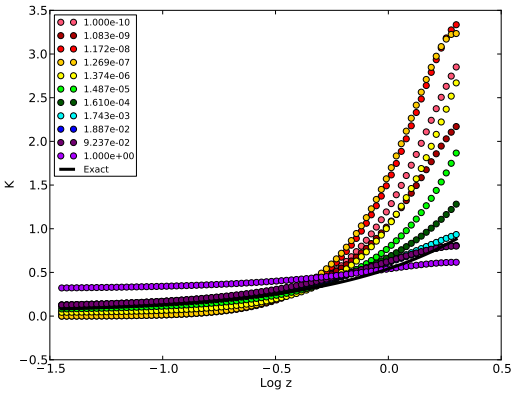


(e) $\lambda = 0.75$ kernel edge

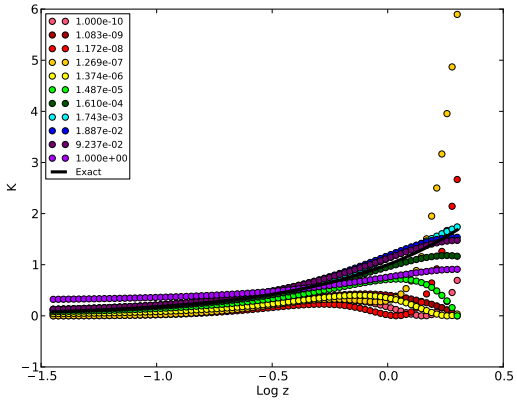


(f) $\lambda = 0.75$ kernel diagonal

Figure 4.2: Inversions from Monte Carlo data, $\lambda \in \{0.25, 0.50, 0.75\}$.

## 4.3 Limitations of Kernel Function Representation Using a Laguerre Polynomial Basis

We conducted some numerical comparisons of the capacity of the Laguerre polynomials to fully represent sum kernel functions with a fractional homogeneity. Using the same discretisation as earlier, and the same number of basis functions in each direction, it is straightforward to apply a Least-Squares approach to obtain the set of parameters that provide the best fit of,

$$\min_{\mathbf{a}} \|\bar{\mathbf{K}} - \mathbf{L}\mathbf{a}\|^2 \tag{4.30}$$

Where $\mathbf{L}$ is the matrix of Laguerre polynomial basis function products $l_n(x,y)$ for all (scaling) kernel coordinates $(x,y)$, and $\bar{\mathbf{K}}$ is the true kernel in vector form with the same ordering of the coordinates. Applying *Mathematica*$^{\text{TM}}$ `NMinimize` to this problem yields a set of parameters $\hat{\mathbf{a}}$ that, when used in $\mathbf{L}\hat{\mathbf{a}}$, are indicative of the best representation of the kernel possible using this combination of orthogonal basis functions and minimisation method. Given the estimated parameters $\hat{\mathbf{a}}$ we can calculate the minimal pointwise errors for kernels with various fractional values of the homogeneity exponent $\lambda$ by comparison of the estimated kernels with the true kernels.

In Figure 4.3 we show the absolute relative errors obtained for kernels with fractional homogeneity exponents $\lambda \in \{0.125, 0.25, 0.375, 0.5, 0.625, 0.75, 0.875\}$. The plots broadly confirm the suspicion that in the region of $\lambda = 0.25$ the approximately 10% relative errors in the representations are sustained into the higher values of $z$ more than for the other values. In addition the plots show that as $\lambda$ is increased the relative errors at small values of $z$ increase towards 60%. Keeping the discretisation fixed at the 80 logarithmically spaced

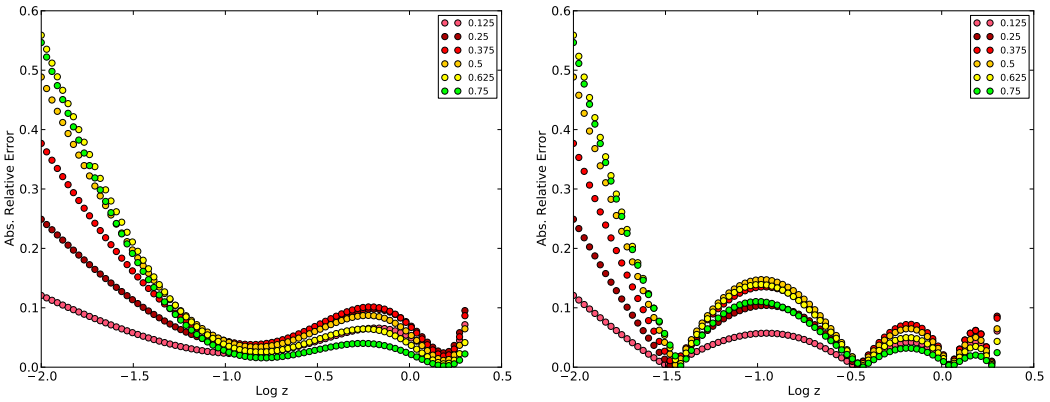


(a) Absolute relative error of the kernel edge

(b) Absolute relative error of the kernel diagonal

Figure 4.3: Absolute relative error of optimal sum kernel representation using Laguerre polynomials for fractional homogeneity exponents, $\lambda \in \{0.125, 0.25, 0.375, 0.5, 0.625, 0.75, 0.875\}$

points recommended in Wright and Ramkrishna [1992] but doubling the number of basis functions to $n_{\text{basis}} = 8$ reduced the relative error at very small $z$ down to approximately 15%, but only halved the relative error to roughly 5% elsewhere. (Predictably, keeping $n_{\text{basis}} = 4$ but doubling the resolution of the discretisation had no effect, giving errors identical to those seen in figurename 4.3.)

## 4.4 Discussion

Though the Wright and Ramkrishna [1992] paper does not assert this very clearly, there are indications that the method is designed to be used iteratively, in conjunction with repeated forward simulations, to gradually refine estimates of kernel functions. (The additional formula for estimating $W$ given in Wright and Ramkrishna [1992, eqn. 38] would then assume more importance.) However, much of the machinery given in the paper for *a posteriori* estimation of $\rho_{\text{reg}}$ would then also seem somewhat superfluous, since contemporary software will run (forward problem) ODE integrations of the SCE quickly. In this case,

the role of the overall method, and its regularisation, is seen to act as a way to reduce the space of possible kernels that need to be tested, not as a clean inversion process. A great deal then hinges on whether the objective is to return pseudo-kernels that reproduce the forward problem reasonably accurately, even though the pseudo-kernels may not resemble the original kernel function well, or whether a reasonably accurate estimate of the original kernel is also required. It is not clear that the Wright and Ramkrishna [1992] method can guarantee to match this latter criterion.

As noted in Connaughton and Jones [2011] the inverse method is very sensitive to the quality of the curve fitting to data for $\Phi(z)$, which raises deeper issues about the value of the results obtained in respect of regularisation. While the original Wright-Ramkrishna method did not appear to work well when used in contemporary mathematical software minimisations, our modified Wright-Ramkrishna method still suffers from two important drawbacks. The first issue, common to both methods, is an inability to represent kernels with fractional exponents to a desirable degree of accuracy. The second is that modifying the regularisation to make the minimisations (seemingly) effective appears to undermine the L-Curve method; hence if the original kernel is unknown, one of the simplest methods for estimating the optimal regularisation parameter value is not accessible and cannot be used to select a good fit to the true kernel. Hence we also do not escape a need to use the method iteratively as suggested above.

The new method developed in Chapter 5 avoids these issues of representation and regularisation choices.

# Chapter 5

# Factorisation of Homogeneous Kernel Functions and Inversion

## 5.1 Introduction

In this chapter, we present a novel inverse method for use against finite stationary case, and finite scaling decay case, mass size distributions which copes readily with fractional kernel exponents. Stationary mass distributions, $N(m)$, result from combining a constant source of monomer masses, $m_0$, injected at a rate $J$, with a finite upper mass size cutoff, $M$, beyond which mass is discarded from the system. A certain amount is already known about the properties of such stationary distributions because the stationary form of the Smoluchowski Coagulation Equation (SCE) [Smoluchowski, 1917] can be analytically solved for a broad class of scale invariant kernels [Hayakawa, 1987][Connaughton et al., 2004]. However, we are not aware of any prior work concerning the use of inverse methods upon this type of distribution. Our work suggests that in this case suitable inverse methods represent a powerful option for obtaining useful kernel function information. We demonstrate that the use of a kernel factorisation scheme can permit the retrieval of a broad class of collision ker-

nels from data without strong prior constraints on their functional form. We also show that this method extends quite well to dealing with data from scaling decay case distributions, $\Phi(z)$.

In §5.2 we briefly discuss the SCE, and detail the factorisation of kernel functions used to generate the parameterised model used in inversions. In §5.3, after a brief discussion of the two main regimes of stationary solutions of the SCE, we show how a Least-Squares method can also be used to generate stationary distributions in both regimes for a key form of kernel. §5.4 then provides the general form of the objective function used in the Least-Squares method for estimating kernel functions from stationary distribution data. In §5.5 we show the extension of the overall method to work with scaling decay distribution data. §5.6 provides our results, including, where necessary, discussion of the trivial adaptations used to extend the power of the factorised kernel representation to handle specific difficult cases. Finally, §5.7 presents our conclusions and suggestions for further work.

## 5.2 The Smoluchowski Coagulation Equation and Kernel Functions

We begin by recapping some general properties of the SCE, using the decay case forward problem as a starting point. In the decay case forward problem the aggregation system is prepared with an initial size distribution consisting entirely of small masses and it is allowed to evolve (or decay) in time, with masses colliding and aggregating to form larger masses which can in turn aggregate with other masses to form even larger masses, and so on. In the case of infinite initial mass there is no upper mass size limit. But for finite initial mass, a single large mass is the eventual result of the evolution of the system. By presuming suitable rescaling, for theoretical purposes the initial masses are usually considered to be of mass $m_0 = 1$ for convenience.

If the aggregating system is such that spatial correlations between particles are sufficiently weak then collisions between particles can be considered statistically independent and a mean field approach is valid. For the forward decay problem, if the collision kernel, $K(m_1, m_2)$, is known, the evolution of the cluster size distribution, $N(m,t) = N_m(t)$, is described by the SCE:

$$\begin{aligned} \partial_t N_m(t) = \frac{1}{2}\int_0^m dm_1\, K(m_1, m-m_1) N_{m_1}(t) N_{m-m_1}(t) \\ - N_m(t)\int_0^\infty dm_1\, K(m, m_1) N_{m_1}(t) \end{aligned} \tag{5.1}$$

The first integral on the RHS accounts for the increase in the number of masses of size $m$ provided from collisions of smaller masses $m_1$, $m_2$ such that $m_1 + m_2 = m$. The second integral term accounts for the loss of masses of size $m$ absorbed by collisions that form masses larger than $m$.

In this chapter we focus on scale invariant problems for which the kernel is a homogeneous symmetric function of its arguments. Denoting the overall degree of homogeneity by $\lambda$,

$$K(hm_1, hm_2) = h^\lambda K(m_1, m_2) \tag{5.2}$$

Such kernels are important because many physical aggregation processes exhibit homogeneity for some range of scales [Kang et al., 1986]. A model kernel, introduced to aid in the analysis of scaling solutions of the SCE (see e.g. van Dongen and Ernst [1988], Leyvraz [2003]), captures the asymptotic behaviour of the aggregation rates as one mass becomes much larger than the other.

$$K_0(m_1,m_2) = \frac{1}{2}\left(m_1^{\mu}m_2^{\nu} + m_2^{\mu}m_1^{\nu}\right) \tag{5.3}$$

Adopting the convention that $\nu \geq \mu$,

$$K_0(m_1,m_2) \sim m_1^{\mu}m_2^{\nu}, \qquad \text{with } m_1 \ll m_2 \tag{5.4}$$

Clearly, $\lambda = \mu + \nu$. It can be shown that in the mean-field limit if $\lambda > 1$ then the mass distribution $N(m,t)$ will develop an infinite component at a critical time $0 \leq t_c < \infty$, a transition known as gelation [van Dongen and Ernst, 1986]. In order to postpone the extra complications connected with this phenonemon [Ball et al., 2011] throughout the remainder of this paper we concern ourselves with finite (maximum mass size $M \ll \infty$) systems with $\lambda \leq 1$.

Another issue of importance, particularly where stationary mass distributions are concerned, is that of the locality of the solutions for a given kernel. In the regime we describe as one of predominantly *local* interactions between scales [Connaughton et al., 2004], the final form of the stationary distribution is independent of $M \to \infty$, and $|\nu - \mu| < 1$. However, there is also a need to treat data where the regime might be *nonlocal* and $|\nu - \mu| > 1$. Whichever regime holds, provided the data represents stable stationary distributions (c.f. Ball et al. [2012]) a good inverse method should cope.

Some kernels that give rise to stationary distributions have functional forms that are not adequately represented by (5.3) alone. However, we posit that for a large class of these kernels they can be expressed as a product of (5.3) and another function, $F(m_1,m_2)$, which is predominantly constant at small and large masses, and has homogeneity zero. So if $K$ is

a general homogeneous kernel, it can be factored as:

$$K(m_1, m_2) = K_0(m_1, m_2)F(m_1, m_2) \tag{5.5}$$

Since $F$ is homogeneous of degree zero, it can be expressed as a function, $f$, of a single variable $x = m_1/m_2$.

$$F(m_1, m_2) = f\left(\frac{m_1}{m_2}\right) \tag{5.6}$$

The symmetry of $F$ in respect of its arguments implies that $f$ must have the symmetry:

$$f(x) = f\left(x^{-1}\right) \tag{5.7}$$

We will call $f(x)$ the *shape function* of the kernel. When the $x$ coordinate of the shape function is mapped to logarithmic coordinates, the result is a function, say $h(y)$, that is symmetric around zero. Provided that the form of $h(y)$ is sufficiently smooth it can be approximated well by a finite orthogonal function basis such as a Fourier cosine series. Since the domain of the Fourier series is $y \in [-\pi, \pi]$ we use the mapping $x \to y$:

$$y = \pi \frac{\log(x)}{\log(M)} \tag{5.8}$$

$$\Rightarrow h(y) := f\left(\exp\left(\frac{y}{\pi}\log(M)\right)\right) \tag{5.9}$$

The approximation of $h(y)$ by the Fourier cosine series then takes the form:

$$h(y) \approx \tilde{h}(y) = \frac{a_0}{2} + \sum_{r=1}^{n} a_r \cos(ry) \tag{5.10}$$
$$a_r = \frac{2}{\pi} \int_0^{\pi} h(y) \cos(ry) dy$$

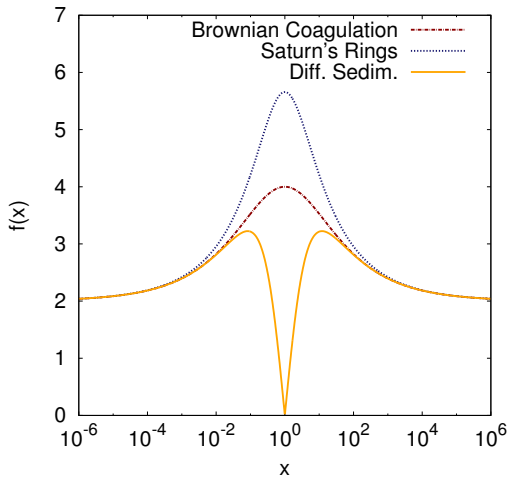


Figure 5.1: The shape functions for the Brownian coagulation kernel, the Saturn's Rings kernel, and the Differential Sedimentation kernel.

Examples of shape functions $f(x)$ for the Brownian Coagulation (continuum regime) kernel, (what we shall call) the Saturn's Rings kernel (see Brilliantov et al. [2009] and references therein) and the Differential Sedimentation kernel, are shown in Figure 5.1. The Saturn's Rings kernel is also known as the Brownian Motion free molecular regime kernel [Aldous, 1999][Smit et al., 1994][1]. These kernels are respectively,

[1] Further details on the origins of the kernel functions used in this chapter can be found in Appendix B.

$$K_{\mathrm{BC}}(m_1,m_2) = (m_1^{\frac{1}{3}} + m_2^{\frac{1}{3}})(m_1^{-\frac{1}{3}} + m_2^{-\frac{1}{3}}) \tag{5.11}$$

$$K_{\mathrm{SR}}(m_1,m_2) = (m_1^{\frac{1}{3}} + m_2^{\frac{1}{3}})^2(m_1^{-1} + m_2^{-1})^{\frac{1}{2}} \tag{5.12}$$

$$K_{\mathrm{DS}}(m_1,m_2) = \left(m_1^{\frac{1}{3}} + m_2^{\frac{1}{3}}\right)^2 \left|m_1^{\frac{2}{3}} - m_2^{\frac{2}{3}}\right| \tag{5.13}$$

To derive the shape function from a known kernel like those above, we form $F = K/K_0$ with the values for $\mu$ and $\nu$ obtained by assuming the asymptotic regime of scaling where $m_1 \ll m_2$ and $K_0(m_1,m_2) \sim m_1^{\mu} m_2^{\nu}$. Using the Saturn's Rings kernel as an example, we obtain $\mu = 2/3,\ \nu = -1/2$ and we then form,

$$F\left(\frac{m_1}{m_2}\right) = \frac{(m_1^{\frac{1}{3}} + m_2^{\frac{1}{3}})^2(m_1^{-1} + m_2^{-1})^{\frac{1}{2}}}{\frac{1}{2}(m_1^{\frac{2}{3}} m_2^{-\frac{1}{2}} + m_1^{-\frac{1}{2}} m_2^{\frac{2}{3}})} \tag{5.14}$$

After some manipulations and setting $x = m_1/m_2$ we obtain the function,

$$f(x) = \frac{2(x^{\frac{1}{3}} + 1)^2(x+1)^{\frac{1}{2}}}{x^{\frac{7}{6}} + 1} \tag{5.15}$$

We can then test our inversions using the Fourier cosine series according to $K = K_0 f(x) \approx K_0 \tilde{h}(y)$. Using a scheme such as this we can then expect to be able to approximate a broad subset of the class of homogeneous kernels.

## 5.3 Stationary Distributions

The generation of a stationary distribution approximates the process in clouds whereby small droplets formed by an ongoing condensation process are driven by air movements

to collide and coalesce to form larger droplets that eventually become heavy enough to overcome updrafts and fall as rain. Because this process forms a stationary distribution, $\partial_t N_m(t) = 0$. The stationary SCE in the presence of a source of monomers is:

$$\begin{aligned} 0 = &\frac{1}{2}\int_0^m dm_1\, K(m_1, m-m_1)\, N_{m_1} N_{m-m_1} \\ &- N_m \int_0^M dm_1\, K(m, m_1)\, N_{m_1} + \frac{J}{m_0}\delta(m-m_0) \end{aligned} \tag{5.16}$$

For kernels in the local regime, with $|\nu - \mu| < 1$, the solution $N_m$ for arbitrary kernels as $M \to \infty$ is known to be of the form [Connaughton et al., 2004]:

$$N_m = A\sqrt{J} m^{-\frac{\lambda+3}{2}} \tag{5.17}$$

Where $A$ is a known constant of proportionality. In the local regime, the distribution is a power law. Whereas in the nonlocal regime when $|\nu - \mu| > 1$ solutions are of the approximate form [Ball et al., 2012]:

$$N_m \approx B\sqrt{J} M^{(m^{-\gamma}-1)} m^{\nu} \tag{5.18}$$

In this case $B$ is a constant of proportionality, $\gamma = \nu - \mu - 1$, and the form of the mass distribution is dependent on the upper cutoff mass size $M$.

It is of course possible to generate stationary distributions for the SCE using numerical ordinary differential equation (ODE) or Monte Carlo integration. However, we have shown in Ball et al. [2012] that for a sufficiently nonlocal kernel of the form in (5.3) the resulting

mass distribution can be dynamically unstable as a function of $M$. Nevertheless, for kernels of this form a simple Least Squares minimisation procedure (shown below), which is similar to work in Dorao and Jakobsen [2006], can be used to generate stationary mass distributions independently of the system dynamics, providing a useful tool for investigations. If it exists, the stationary state is acquired by this method directly, in a manner independent of the evolution of aggregates.

### 5.3.1 Generating Stationary Distributions

The following description echoes that in Ball et al. [2012, Appendix A]. To compress the notation it is helpful to introduce the discrete moments form, $\mathscr{M}_p$:

$$\mathscr{M}_p = \sum_{m=1}^{M} m^p N_m \tag{5.19}$$

Using the discrete form of equation (5.16), and a kernel of the form in (5.3), we can then use the moments form to decompose (5.16) as:

$$N_m = \frac{G + \mathscr{J}}{\left(m^\mu \mathscr{M}_\nu + m^\nu \mathscr{M}_\mu\right)} \tag{5.20}$$

Where,

$$G = \sum_{m_1=1}^{m-1} K_0(m_1, m-m_1)\, N_{m_1} N_{m-m_1} \tag{5.21}$$

$$\mathscr{J} = \frac{2J}{m_0}\delta(m-m_0) \tag{5.22}$$

Setting $m_0 = 1$ gives the first term of the stationary distribution as,

$$N_1 = \frac{2J}{\mathscr{M}_\nu + \mathscr{M}_\mu} \tag{5.23}$$

Given the behaviour of the equation for $G$ this permits a recursive definition of a stationary distribution, if the pair of moments $(\mathscr{M}_\mu, \mathscr{M}_\nu)$ are known.

If $J$, $\mu$ and $\nu$ are known then (5.20) can be used to infer the rest of the stationary distribution by treating the problem as one of parameter estimation. In this case we seek the correct values of the pair of moments $(\mathscr{M}_\mu, \mathscr{M}_\nu)$ which will then generate the correct stationary state distribution. By treating $N_m$ as a function of the pair of moments $N_m(\mathscr{M}_\mu, \mathscr{M}_\nu)$ we can create an objective function $\Psi(\mathscr{M}_\mu, \mathscr{M}_\nu)$ to be minimised.

$$\begin{aligned}\Psi(\mathscr{M}_\mu, \mathscr{M}_\nu) = (\mathscr{M}_\mu - \sum_{m=1}^{M} m^\mu N_m(\mathscr{M}_\mu, \mathscr{M}_\nu))^2 \\ + (\mathscr{M}_\nu - \sum_{m=1}^{M} m^\nu N_m(\mathscr{M}_\mu, \mathscr{M}_\nu))^2\end{aligned} \tag{5.24}$$

$$(\mathscr{M}_\mu *, \mathscr{M}_\nu *) = \arg \min_{(\mathscr{M}_\mu, \mathscr{M}_\nu)} \Psi(\mathscr{M}_\mu, \mathscr{M}_\nu) \tag{5.25}$$

## 5.4 Retrieving Kernels from Stationary Distributions

In general, for the inverse problem, $J$ is not known. However, we presume that it is possible to normalise stationary distribution data such that $J = 1$ is an acceptable assumption. The remaining parameter estimation problem for a kernel of the form in (5.3) is to determine $\mu$ and $\nu$. If we let $\mathscr{R}_m$ stand for the entire right-hand side of (5.16) we can create an objective function $S$ and minimise it to obtain the two parameters.

$$S(\mu,\nu) = \frac{1}{M}\sum_{m=1}^{M} \mathscr{R}_m(\mu,\nu)^2 \tag{5.26}$$

$$(\mu*,\nu*) = \arg\min_{(\mu,\nu)} S(\mu,\nu) \tag{5.27}$$

For more general kernels, we can deploy the factorisation of the kernel in (5.5) into a similar scheme. If we are approximating the shape function by, for example, the Fourier series in (5.10), then an extension of the parameter estimation approach in (5.27) creates an inverse method for retrieving the form of such kernels. In this case the estimated parameters are $\mu$, $\nu$, and the set of coefficients, $\{a_r\}$, $r = 0, ..., n$, of the finite Fourier cosine series.

$$S(\mu,\nu,\{a_r\}) = \frac{1}{M}\sum_{m=1}^{M} \mathscr{R}_m(\mu,\nu,\{a_r\})^2 \tag{5.28}$$

$$(\tilde{\mu},\tilde{\nu},\{\tilde{a}_r\}) = \arg\min_{(\mu,\nu,\{a_r\})} S(\mu,\nu,\{a_r\}) \tag{5.29}$$

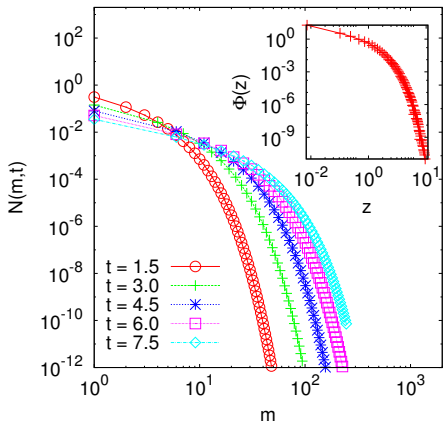


Figure 5.2: An example of a scaling decay case distribution. The main panel shows the time evolution of the distribution for a sum kernel $K(m_1,m_2) = \frac{1}{2}(m_1^\lambda + m_2^\lambda)$ with $\lambda = 0.5$ and $M = 250$; and the inset panel shows the rescaled time invariant distribution.

## 5.5 Retrieving Kernels from Scaling Decay Distributions

A minor modification of the above method permits the estimation of kernel parameters from scaling decay-case mass distribution data (see Figure 5.2). If $\Phi(z)$ is the time-invariant scaled distribution function, where $z = m/s(t)$ and $s(t)$ is the scaling typical mass, then assuming that the scaling relations,

$$N(m,t) = s(t)^{-2}\Phi(z) \tag{5.30}$$

$$s(t) = \frac{\mathscr{M}_2(t)}{\mathscr{M}_1(t)} \tag{5.31}$$

hold [Leyvraz, 2003], we can rearrange the rescaled SCE as,

$$\begin{aligned} 0 = \frac{1}{2}\int_0^z dz_1\, \kappa(z_1, z-z_1)\Phi_{z_1}\Phi_{z-z_1} \\ - \Phi_z \int_0^\infty dz_1\, \kappa(z,z_1)\,\Phi_{z_1} + \left(2\Phi_z + z\frac{d\Phi}{dz}\right) \end{aligned} \tag{5.32}$$

Here, $\kappa(z_1,z_2) = K(z_1,z_2)/W$ , where $W$ is the separation constant of the scaling [van Dongen and Ernst, 1988][Leyvraz, 2003]. We then deploy our kernel estimation process using:

$$\kappa(z_1,z_2) = K_0(z_1,z_2)F(z_1,z_2) \tag{5.33}$$

When data for the time evolution of $N(m,t)$ is available then using (5.31) to generate the scaling distribution in (5.30) is straightforward. However, for some kernels $W \neq 1$ and it must be retrieved by fitting the data curve obtained using (5.31) with the analytic solution

for $s(t)$:

$$s(t) = [(1-\lambda)Wt + X]^{\frac{1}{1-\lambda}}, \quad \lambda < 1 \tag{5.34}$$

Here $X$ is a parameter replacing the initial condition term $s(0)^{1-\lambda}$. Provided that $(\mu, \nu)$ are retrieved sufficiently well during the estimation of the kernel, then the homogeneity $\lambda$ can be inferred from $\mu + \nu = \lambda$ and given this the fitting process to obtain $W$ works well. Multiplying the retrieved kernel estimate $\kappa(z_1, z_2)$ by $W$ rescales the result to match the original unscaled input kernel $K(z_1, z_2)$.

Presuming that our $\Phi(z)$ conform to (5.30) sufficiently well, we can once again deploy the parameter estimation minimisation technique found in (5.29), but modified to use a judicious choice of discretisation of the $z$ dimension. With $\mathscr{R}_z$ as the entire right-hand side of (5.32), and $Z$ as the number of discretisation points between $z_{\min}$ and $z_{\max}$, we use,

$$S_\Phi(\mu, \nu, \{a_r\}) = \frac{1}{Z} \sum_{z=z_{\min}}^{z_{\max}} \mathscr{R}_z(\mu, \nu, \{a_r\})^2 \tag{5.35}$$

$$(\tilde{\mu}, \tilde{\nu}, \{\tilde{a}_r\}) = \arg \min_{(\mu, \nu, \{a_r\})} S_\Phi(\mu, \nu, \{a_r\}) \tag{5.36}$$

We remark that we suspect that this approach is more likely to work for kernels in the local regime where the scaling hypothesis holds more strongly but that we have as yet been unable to confirm this convincingly.

## 5.6 Results

### 5.6.1 General Remarks

It is necessary to remark on the minimisation methods used. Throughout, the minimisations were done in *Mathematica*™ v.8 using its `NMinimize` function. However, it was found that for small values of $n \leq 2$ the Nelder-Mead method produced retrieved parameters values resulting in better fits, whereas for values $n > 2$ the Differential Evolution method worked better. The results shown were obtained by running the minimisations with both methods and then selecting the better set of results.

### 5.6.2 Stationary Distribution Results

We performed a structured series of tests to ascertain the properties of the new method. The individual components of the method were first tested separately, followed by tests on the full method.

First, we found that (stable) stationary distributions produced by the minimisation method (from §5.3.1) and using the kernel form in (5.3) were sufficiently equivalent to those (that are asymptotically stable in time) produced from ODE integration. Differences were the same order of magnitude as the chosen error margin of the minimisation process.

The parameter estimation method in (5.27) was then applied to stationary distributions with $M = 250$ generated using the kernel form in (5.3) with system size $M = 250$. The original exponent value pairs, shown as $(\mu, \nu)$ in (5.3), were in the set $P = \{(p_i, p_j) : j \geq i;\ p_i, p_j \in X\}$ with $X = \{-0.75, -0.50, -0.25, 0, 0.25, 0.50, 0.75\}$. These tested cases cover a broad range of local and nonlocal kernels with fractional exponent values. The retrieval of the kernel exponent values was very accurate in all cases, reproducing the exponents to at least 2 decimal places, commensurate with the input values.

| Brownian Coagulation Kernel | | | | | |
|---|---|---|---|---|---|
| Known | | | Estimated | | |
| M | $\mu$ | $\nu$ | $\hat{\mu}$ | $\hat{\nu}$ | $\hat{C}$ |
| 100 | 1/3 | -1/3 | 0.24 | -0.24 | 4.00 |
| 250 | 1/3 | -1/3 | 0.24 | -0.24 | 4.00 |
| Saturn's Rings Kernel | | | | | |
| Known | | | Estimated | | |
| M | $\mu$ | $\nu$ | $\hat{\mu}$ | $\hat{\nu}$ | $\hat{C}$ |
| 100 | 1/3 | -1 | 0.51 | -0.35 | 5.67 |
| 250 | 1/3 | -1 | 0.52 | -0.36 | 5.67 |

Table 5.1: Results for the attempted estimation of just the bulk exponents for the Brownian Coagulation and Saturn's Rings kernels. The bulk exponents are not well estimated, and the value of the constant $\hat{C}$ is well within the non-asymptotic regime of the kernel.

We then tested whether the substitution of the kernel form in (5.3) for the bulk behaviour of selected non-factorisable kernels (the Brownian Coagulation and Saturn's Rings kernels) worked well. In these cases shape function approximation was reduced to estimating a simple constant, $C$, as a multiplier of (5.3), so that the estimating kernel form, $K_E$, is given by:

$$K_E(m_1,m_2) = \frac{\hat{C}}{2}\left(m_1^{\hat{\mu}} m_2^{\hat{\nu}} + m_2^{\hat{\mu}} m_1^{\hat{\nu}}\right) \tag{5.37}$$

Estimation of the bulk exponents for selected non-factorisable kernels at first sight seemed poor. See Table 5.1. In particular the estimated values for the constant $\hat{C}$ strongly reflect the behaviour of the maximum of the shape function when $x = 1$, well within the (local) non-asymptotic regime of the kernel. This was unsurprising given the limited maximum mass size $M = 250$ of the simulated distributions, as on the logarithmic scale most of the data points are in the vicinity of the peak.

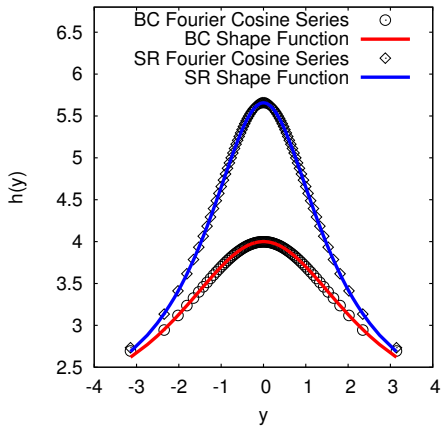


Figure 5.3: Comparisons between the known shape functions $f(x) \to h(y)$ and the retrieved Fourier cosine series estimations, $\tilde{h}(y)$, for the Brownian Coagulation and Saturn's Rings kernels. The discrete points for the Fourier series curves are the points obtained from $x = m_1/m_2$ when the masses have integer values. System size was $M = 250$.

In order to test whether the cosine Fourier series approximation of the shape function works well in isolation, within the parameter estimation process we fixed $(\mu, \nu)$ to their correct values and then attempted to estimate the Fourier coefficients for approximating the shape function. For the Brownian Coagulation and Saturn's Rings kernels this worked well, and the results are shown in Figure 5.3.

We then combined the use of the kernel form in (5.3) with the cosine Fourier series approximation from (5.10). The number of Fourier coefficients was arbitrarily set with $n = 4$. (Hence, including $r = 0$, there were 5 Fourier coefficients in total.)

For the Brownian Coagulation and Saturn's Ring kernels, with data for $M = 250$, parameter estimates for the bulk exponents and the Fourier coefficients of the shape function were obtained. Although neither the retrieved bulk exponents values nor the fitted shape function matched the input kernel parameters and shape function well, when the retrieved parameters were fed back into the forward problem (using ODE integration) excellent fits to the origi-

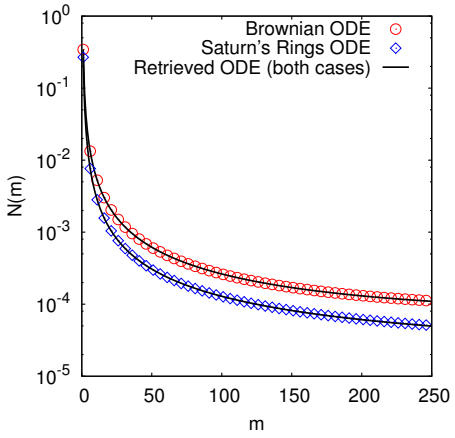


Figure 5.4: Comparisons between the original stationary distributions, for the Brownian Coagulation and Saturn's Rings kernels, and their approximation using the pseudo-kernels generated by the combined parameter estimation process in (5.29). System size was $M = 250$.

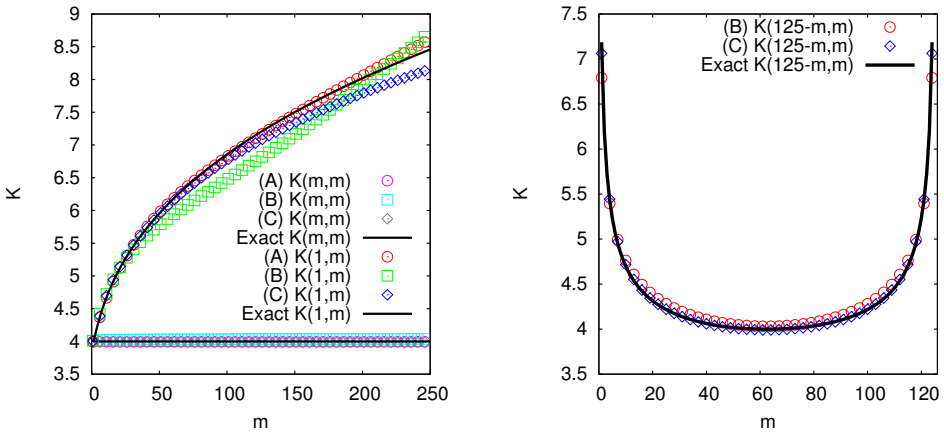


Figure 5.5: Comparisons between the original Brownian Coagulation kernel (black lines), (A) the calculated optimal representation possible using a truncated Fourier cosine series with $n = 4$, and the retrieved kernels generated by the combined parameter estimation process in (5.29) with (B) $n = 4$ and (C) $n = 0$. System size was $M = 250$. The left panel compares the edges, and similarly the diagonals, of the kernel and the different estimations. The right panel compares the true kernel with the retrieved estimations (B) and (C) for a cross-section along the line $m_1 + m_2 = 125$.

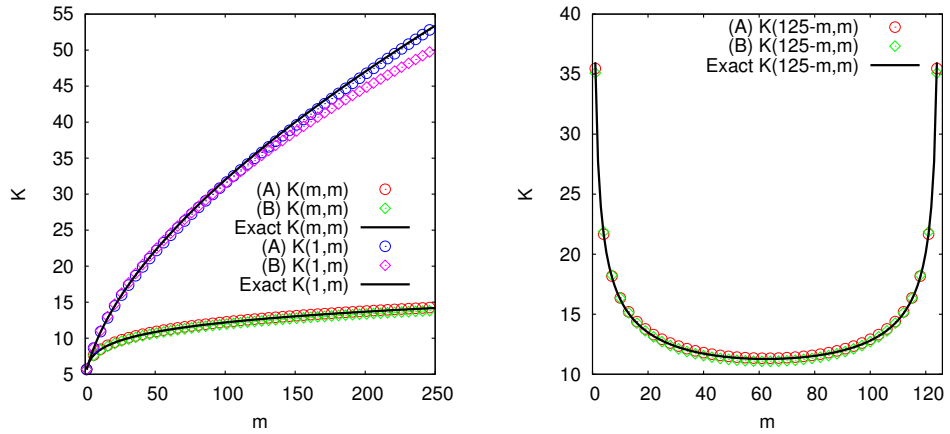


Figure 5.6: Comparisons between the original Saturn's Rings kernel (black lines) and the retrieved kernel generated by the combined parameter estimation process in (5.29) with (A) $n = 4$ and (B) $n = 0$. System size was $M = 250$. The left panel compares the edges, and similarly the diagonals, of the kernel and the estimations. The right panel compares the true kernel with the retrieved estimations (A) and (B) for a cross-section along the line $m_1 + m_2 = 125$.

nal stationary distributions were obtained, as shown in Figure 5.4. The mean and pointwise maximum differences between the original and approximated stationary distributions for both kernels were also suitably small, being of the order of $10^{-6}$ or less.

When the combined parameter estimation method of (5.29) was applied to the stationary distribution for the Brownian Coagulation kernel, the retrieved kernel function was found to approximate the original kernel well. In Figure 5.5 (left panel) it can be seen that the form of the retrieved kernel is to some extent governed by the use of a truncated Fourier series with $n = 4$, with the pattern of error along the kernel edges tracking that of the optimal representation (using the known exact exponents and calculable Fourier coefficients) of the original kernel using a truncated Fourier cosine series of the same length. Even better results were obtained for the Saturn's Ring kernel, as shown in Figure 5.6.

We then tested whether the combined parameter estimation method would work on a generalisation of the Brownian Coagulation kernel with $\mu = \alpha,\ \nu = -\alpha$. We generated stationary distributions (using ODE integrations) with $\alpha \in \{0.00, 0.25, 0.50, 0.75\}$. After applying the combined minimisation method with $n = 4$, the retrieved parameters were used to generate approximating stationary distributions using ODE integration. In all these cases of $\alpha$ the fits between the original stationary distributions and the approximating ones were also very good, with differences from the original distributions being of the order of $10^{-5}$ or smaller.

When the same parameter estimation results were used to generate retrieved kernel functions it was found (see Figure 5.7, left figure) that the approximation was very good in all cases except for $\alpha = 0.00$. In this last case the Fourier approximation overshoots significantly at the edges, as is shown in the right panel of Figure 5.7. In fact, for this case the best fit was obtained with only one Fourier coefficient, $a_0$.

We also tested the method against the Differential Sedimentation kernel (5.13), which has a shape function with a cusp in the centre. In this case the approximation of the shape function by a finite Fourier cosine series did not perform at all well, and a good approximation to the kernel was not obtained. However, it was found that by mapping both sides of the shape function to the positive interval $[0, \pi)$ and instead approximating the shape function using a full (sine and cosine) Fourier series with $n = 3$,

$$y^+ = \pi \frac{|\log(x)|}{\log(M)} \tag{5.38}$$

$$\Rightarrow h_+(y^+) := f\left(\exp\left(\frac{y^+}{\pi}\log(M)\right)\right) \tag{5.39}$$

$$\approx \tilde{h}_+(y^+) = \frac{a_0}{2} + \left[\sum_{r=1}^{n} a_r \cos(ry^+) + b_r \sin(ry^+)\right] \tag{5.40}$$

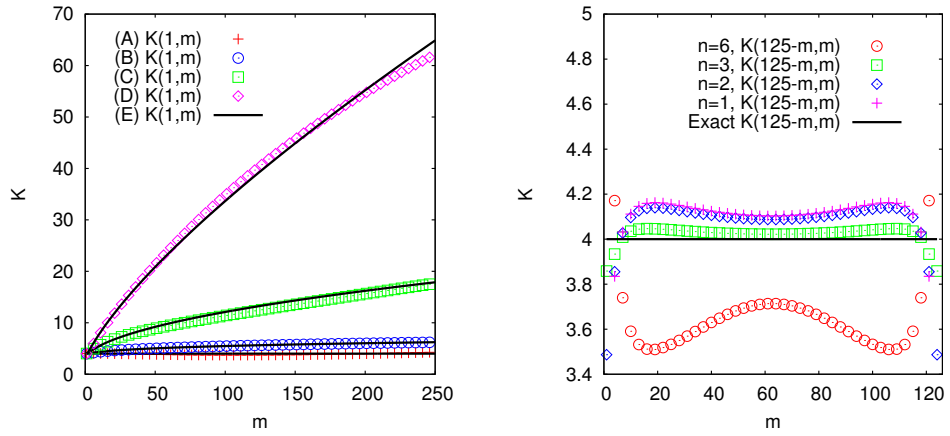


Figure 5.7: Comparisons between the Generalised Brownian Coagulation kernel with $\alpha = \{0.00, 0.25, 0.50, 0.75\}$ (black lines, case (E)) and the approximations (A) $\alpha = 0.00$, (B) $\alpha = 0.25$, (C) $\alpha = 0.50$, (D) $\alpha = 0.75$, using the retrieved kernels generated by the combined parameter estimation process in (5.29) with $n = 4$. System size was $M = 250$. The left panel compares the edges of the kernels and their estimations. The right panel compares the true kernel for $\alpha = 0.00$ with the retrieved estimations for a cross-section along the line $m_1 + m_2 = 125$ for different values of $n$.

With a weighted objective function,

$$S_{\mathrm{FF}}(\mu, \nu, \{a_r\}) = \sum_{m=1}^{M} \frac{\mathscr{R}_m(\mu, \nu, \{a_r\})^2}{N(m)} \tag{5.41}$$

an excellent approximation to the kernel could be obtained, as is shown in Figure 5.8. The absence of a $1/M$ prefactor in (5.41) is based upon testing. We conjecture that there is a relationship between the precision goal of the minimisation and the approximation of the zero point in the shape function cusp that benefits from the removal of this factor.

While this approach using a full Fourier series works for the Differential Sedimentation kernel, it did not work well for the Brownian Coagulation and Saturn's Rings kernels. Hence the power of the overall minimisation scheme to adequately match certain classes of kernels remains dependent upon the choice of orthogonal basis functions used to represent

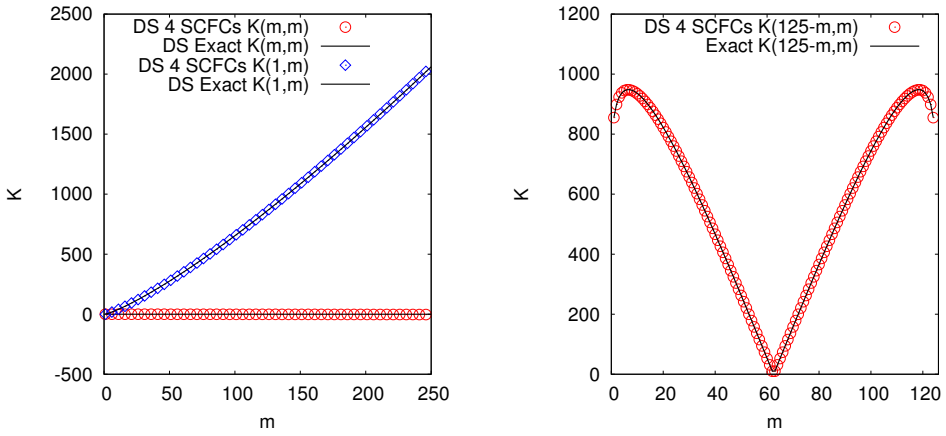


Figure 5.8: The left panel shows the edges and diagonal of the estimates of the Differential Sedimentation kernel function produced when the shape function mapped to $[0,\pi)$ is approximated by a full (sine and cosine) Fourier series with $n = 3$, as compared with the true kernel (black lines). The right panel compares the true kernel (black line) with the retrieved estimations for a cross-section along the line $m_1 + m_2 = 125$. System size was $M = 250$.

the shape function.

### 5.6.3 Scaling Decay Distribution Results

We then sought to ascertain whether the method would perform similarly well against scaled mass distributions generated from the scaling decay case. A comparison with the method tested in Connaughton and Jones [2011] provided a good starting point.

For each of the sum kernels,

$$K(m_1, m_2) = \frac{1}{2}\left(m_1^\lambda + m_2^\lambda\right) \tag{5.42}$$

with $\lambda \in \{0.0, 0.25, 0.5, 0.75, 1.0\}$ we used ODE integration with $M = 250$ to generate approximately scaled distribution data. A function consisting of a sum of (1 or 2) Gamma distributions was fitted to the scaled distribution data for each case of $\lambda$ using a regression

method to obtain an estimated scaling function $E(z)$. We then substituted $E(z)$, replacing $\Phi(z)$, into the method in (5.36) to obtain an estimated kernel parameterisation. We set the discretisation lower limit $z_{\min} = 0.01$ and chose a fixed discretisation increment to be $\Delta z = 0.01$ for convenience. The results of inversion were found to be sensitive to the quality of fit for the tail of $E(z)$. With the larger values of $\lambda$, at larger values of $z$ the scaling did not necessarily conform to matching a sum of Gamma distributions, hence this affected the quality of fit of $E(z)$ in the region of larger $z$. Therefore, for consistency, the upper limit of the discretisation was restricted to $z_{\max} = 2.0$ to select that subset of the data for which the fit for $E(z)$ qualitatively appeared to hold well in all cases. This matches the choices of lower and upper limits of discretisation used in Wright and Ramkrishna [1992]. Our tests also indicated that (using our approach to generating the scaling distributions) $W = 1$ for these kernels.

Initially, the kernel in (5.37) with a single Fourier coefficient, $a_0 = \hat{C}$, was used in the retrieval process. Overall, the results (shown in Figure 5.9) for all values of $\lambda$ used were promising. While the two cases of $\lambda = 0.00$ and $\lambda = 1.00$ were recovered well, for the kernels with fractional values of $\lambda$ there was a consistent pattern of relatively minor deviation from the true kernels.

Tests indicated that it was possible to reduce the amount of deviation of the retrieved (fractional exponent) kernels by improving the fit of $E(z)$ against a larger set of data with $2.0 \leq z_{\max} \leq 3.0$. The quality of the scaling of the data also impacted upon the quality of fit of $E(z)$. It is therefore likely that much of the potential for deviation arises in the sensitivity of the fitting process for $E(z)$ and not in the main inversion process. Later tests against larger decay case evolutions with improved scaling added additional support for this view.

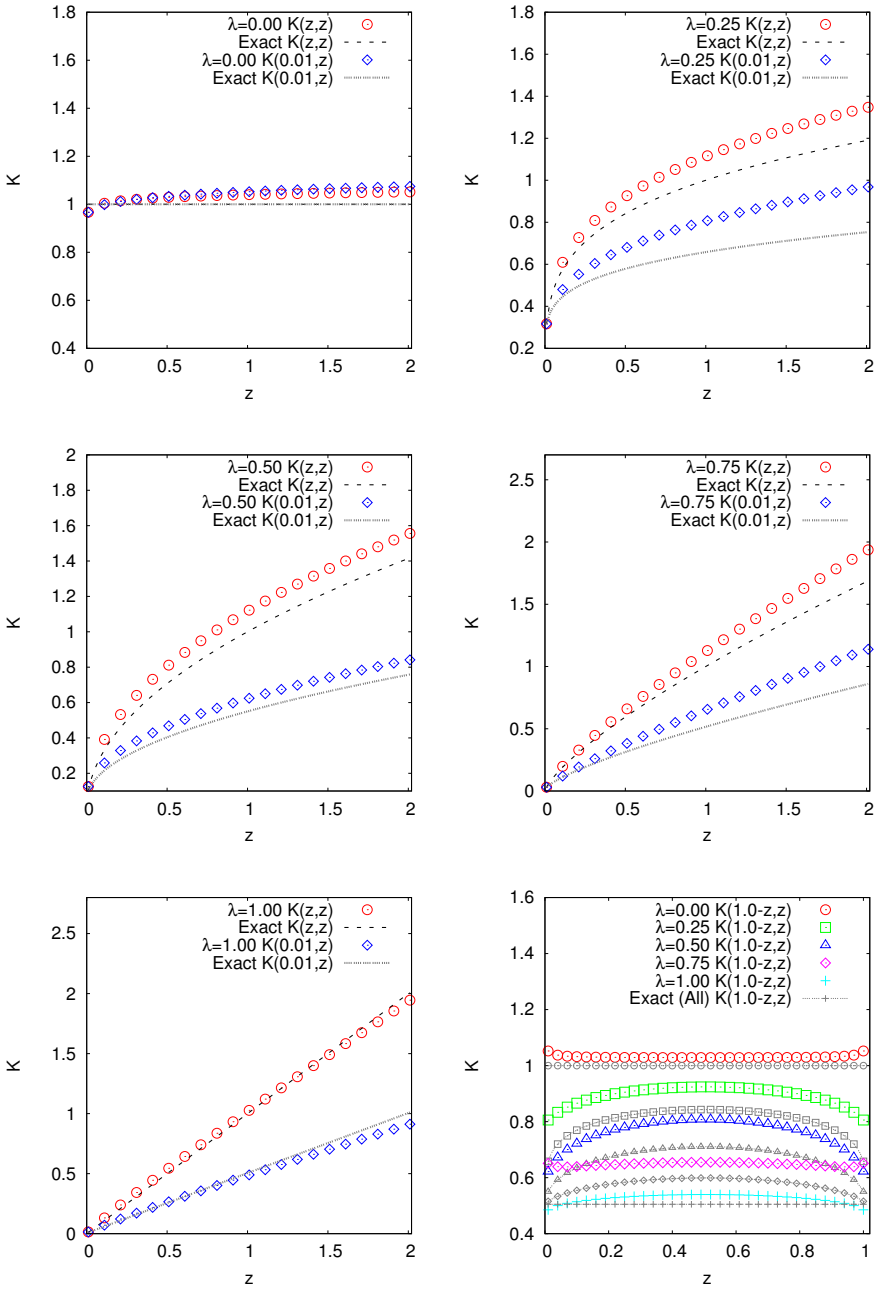


Figure 5.9: Comparisons of the kernels estimated from decay-case scaling distributions generated using kernels of the form in (5.42), with $\lambda \in \{0.00, 0.25, 0.50, 0.75, 1.00\}$. Five of the plots show the edges and diagonals of the retrieved kernels compared with those of the exact kernels. The sixth plot shows comparisons for a suitable cross-section line for all kernels. (Estimates match against the respective grey lines with similar symbols.)

We remark that for these known input sum kernels, a coincidental by-product of this kernel fitting configuration with a single Fourier coefficient is that one of the estimated kernel exponents ($\hat{\mu}$ or $\hat{\nu}$) will be close to zero, and the other close to $\lambda$ when $\hat{C} \approx 1$. Of course, when the input kernel is unknown, the fitting configuration does not in general have any extra meaning. However, it might be supposed that since ultimately $\hat{C} \approx 1$, and since the sum kernels are a subclass of the kernel in (5.3) that this scalar multiplier could be removed from the fitting model without harm. Contrary to this idea, we found in tests that removing the single Fourier coefficient had a considerable adverse affect on the quality of fit for all $\lambda$ values. For comprehensiveness, we also tested fitting with 2 Fourier coefficients, but found no clear improvement upon the fits using just one Fourier coefficient.

Since the results for the sum kernel cases were promising, we then tested the same inversion process upon a set of approximately scaling distributions generated using the kernel form in (5.3) and $M = 250$. We chose as representative examples two kernels with $(\mu, \nu) \in \{(-0.25, 0.50), (-0.75, 0.50)\}$. We set $z_{\min} = 0.05$ and set the number of discretisation points to $Z = 100$. Owing to variations in the quality of the scaling of the distribution data $z_{\max}$ was varied from a minimum of 2.5 for the first case, up to 6.0 for the second case. Unfortunately, initial results were all very poor.

However, by modifying the method to use a weighted form of the objective function ($\hat{S}_\Phi$ as shown below) it was found that it was possible to obtain a good estimate for the $K(z, z)$ centre line of these kernels. Once again, for comprehensiveness, we also tested fitting with 2 Fourier coefficients, but found no clear improvement upon the fits using just one Fourier coefficient.

$$\hat{S}_\Phi(\mu, \nu, \{a_r\}) = \frac{1}{Z} \sum_{z=z_{\min}}^{z_{\max}} \frac{\mathscr{R}_z(\mu, \nu, \{a_r\})^2}{\Phi(z)} \tag{5.43}$$

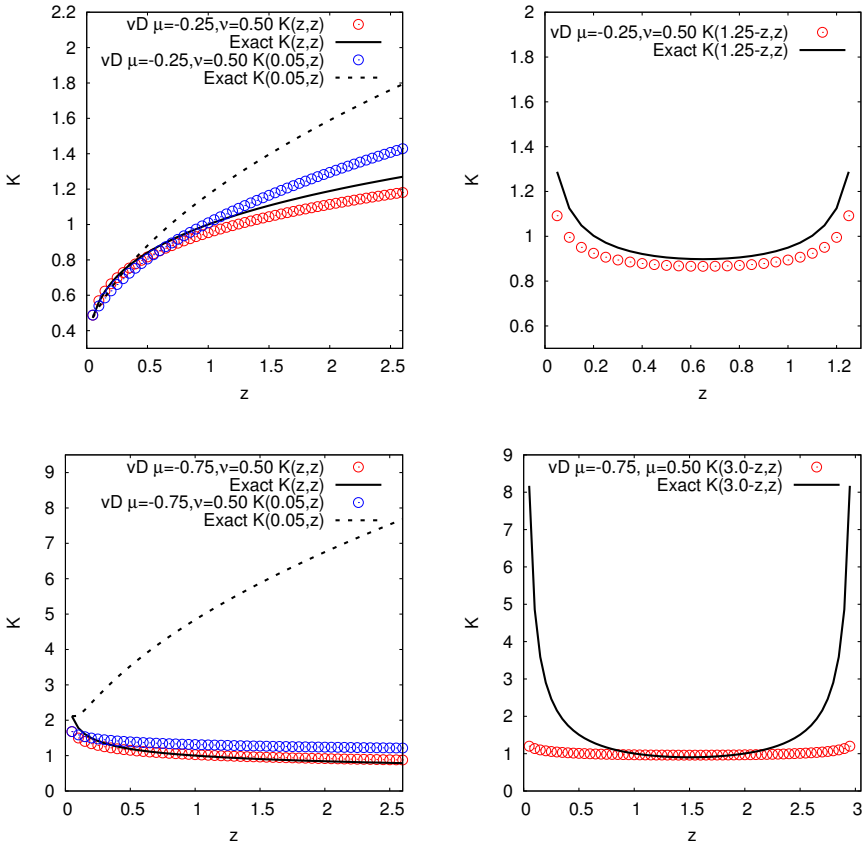


Figure 5.10: Plots showing the kernels estimated from decay-case scaling distributions generated using kernels of the form in (5.3) with $(\mu, \nu) \in \{(-0.25, 0.50), (-0.75, 0.50)\}$. For each pair, the left plot shows the edges and diagonals of the retrieved kernels compared with those of the exact kernels. The right plot shows a similar comparison for a suitable cross-section line. "vD" is short for "van Dongen", a reference to one of the originators of the kernel form in (5.3).

These results are shown in Figure 5.10. Interestingly, we were able to obtain a good estimate of $K(z, z)$ even for the case of $(\mu, \nu) = (-0.75, 0.50)$ despite this case being in the nonlocal regime.

Lastly, we used ODE integration to generate scaling distributions, with $M = 250$, for the Brownian Coagulation kernel, the Saturn's Rings kernel, and in addition, the Shear

(Nonlinear Velocity Profile) kernel [Aldous, 1999][Smit et al., 1994]. This latter kernel is,

$$K_{\mathrm{SNLV}}(m_1, m_2) = \left(m_1^{1/3} + m_2^{1/3}\right)^{7/3} \tag{5.44}$$

For these kernels $W \neq 1$ and it must be inferred from the data in each case. The results, for inversions with one Fourier coefficient, are shown in Figure 5.11. (Using two Fourier coefficients did not improve the fits.) Again, the $K(z, z)$ centre lines of the kernels were retrieved well, but there is some deviation at the edges.

## 5.7 Discussion

For stationary distributions, while the full minimisation method does not retrieve the exact parameter values for known inputs, because there is some transfer of value between the $K_0$ kernel exponents and the Fourier coefficients, it nevertheless obtains parameter values which recover a broad class of kernels very well. These kernels can then also be deployed in the forward problem to recover the stationary distributions for this class of kernels with considerable accuracy.

With a minor adaptation of the method to use a full Fourier series in the kernel factorisation it also became possible to estimate the Differential Sedimentation kernel with remarkable accuracy. Though this departs from being able to deploy only a single general method, there is little extra cost in deploying both the core method and this adaptation and then subsequently evaluating which estimated kernel performs best in the forward problem of recreating the input data. Our tests suggested that it is likely that only one will perform well in a given case. Such adaptations are equivalent to adding stronger prior information about the kernel to the inversion process. However, we remark that when the shape function

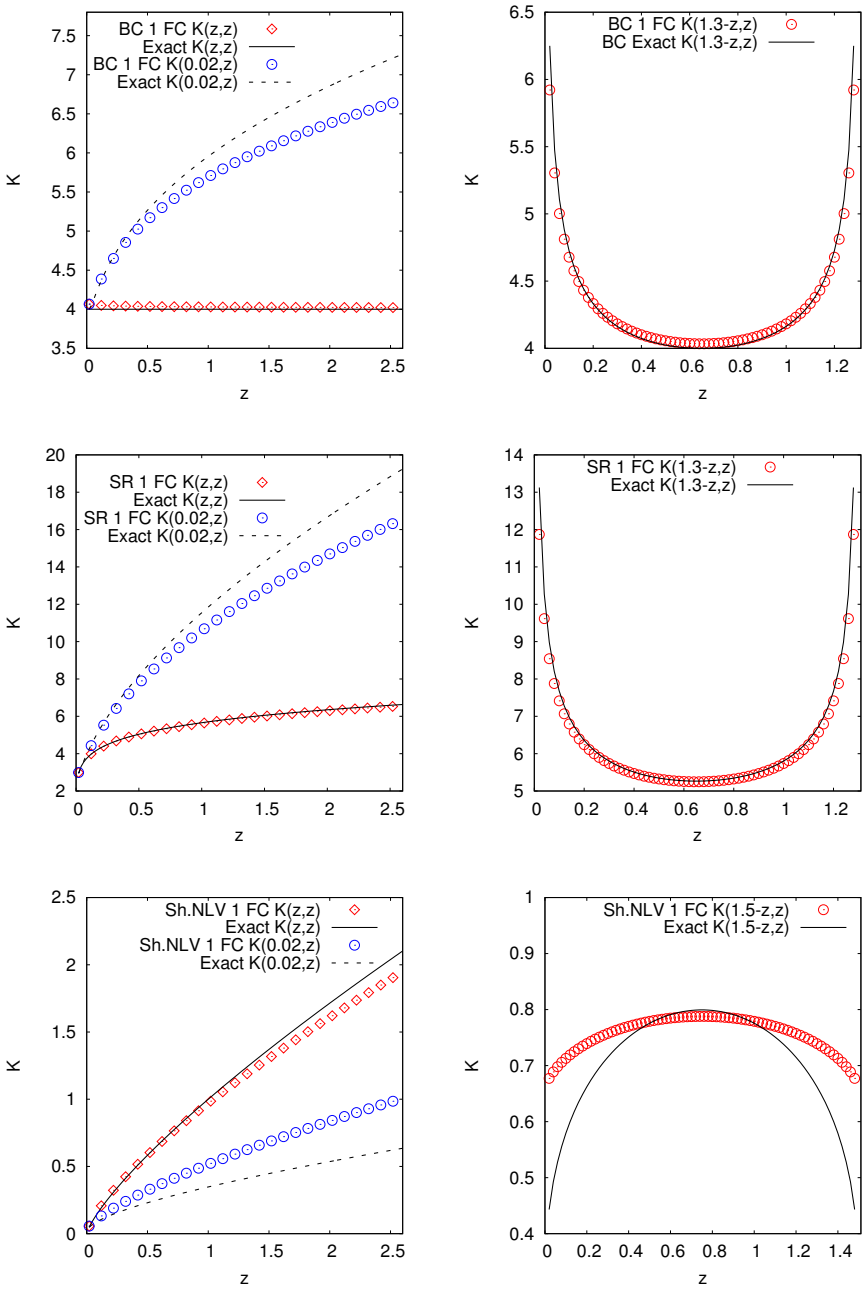


Figure 5.11: Pairs of plots showing the kernels estimated from decay-case scaling distributions generated by the Brownian Coagulation, Saturn's Rings, Shear (Nonlinear Velocity Profile) kernels, respectively. Each left panel shows the edges and diagonals of the retrieved kernels compared with those of the exact kernels. Each right panel shows a similar comparison for a suitable cross-section line.

$f(y)$ for the Differential Sedimentation kernel is mapped as $g(y) = |f(-y)|$, the resulting shape function lacks a cusp, yielding a 'nice' shape function, like that of the Brownian Coagulation kernel. This raises the possibility that, under suitable generalisation, the kernel factorisation method might be able to match a wider class of kernels without prior adaptations.

With a simply weighted adaptation of the new method, the quality of estimated kernels obtained from scaling decay case distribution data for sum kernels with fractional exponents is superior to that obtained using the method in Chapter 4 and our earlier paper [Connaughton and Jones, 2011]. We contend that our new method is also significantly simpler to apply and less computationally demanding than that of Wright and Ramkrishna [1992].

However, for the $K_0$ kernels only the $K(z,z)$ centre lines were retrieved well. One hypothesis was that this might be a consequence of our input distribution not conforming sufficiently well to the large mass, large time, requirements of the scaling hypothesis, and hence the asymptotic values of $(\mu, \nu)$ are not adequately distinguished even though $\lambda$ can be acquired. However, further tests with large system sizes where scaling is more precise yielded no change in the inversions, suggesting that the real problem lies with the sensitivity to the fitting quality of $E(z)$. Further work is needed to establish whether this is the case.

Lastly, we have demonstrated that for specific well-known kernels, reasonable estimates can be obtained from approximately scaling decay case distribution data.

Further work would include investigating whether the method could also be extended to tackle non-scaling, non-stationary $N(m,t)$ distribution data, and investigating the robustness of the method when confronted with data affected by noise.

# Chapter 6

# Conclusions and Outlook

As noted in the introduction, there exist a number of key problems in physics for which analytic and computational methods remain severely constrained. A detailed and complete exposition of the lifecycles of clouds remains one such area requiring concerted research. A full description of the microphysics of clouds is currently lacking owing to their complexity, not only because of the role of turbulence across almost the full range of scales involved in a cloud, but also because of the myriad feedback relationships both within clouds and within the meteorology and planetary climate of which they are a part. Local changes to key microphysical processes affecting cloud activity, including the increase in the uptake of man-made aerosol particles, the effect of chemical and temperature changes on the rate of formation of micro-droplets through condensation processes, and the rate of aggregation of droplets to form raindrops or snowflakes, can have significant feedback effects into overall climate trends. Likewise, changes in overall climate trends can feed back into changes in microphysical activities that are constitutive of clouds.

Despite the constraints upon analytic and computational methods at present, improved instrumentation and enhanced observations of cloud properties are providing essential data which can be analysed to provide complementary support to other methods. Notably, im-

proved observations of the evolution of the cloud droplet size distributions, $N(m,t)$, could enable crucial comparisons between empirical studies and simulation studies to be made. Better understanding of the micro- and macroscale processes of clouds can in turn be used to improve the accuracy of the projections of global climate models, which in turn will improve the information provided to policymakers.

Elsewhere, in industrial applications, more efficient methods enabling real-time monitoring, control, and adaptation of certain processes involving aggregation of particles remains a goal. Chemical mixing and surface deposition (epitaxial) processes are in this class. Faster and better inverse methods should provide a more concerted link between improved instrumentation, observations, and process control.

The research in this thesis was undertaken with such goals in mind. We set out to demonstrate that it was possible to develop robust new inverse methods capable of retrieving adequate representations of homogeneous kernels with fractional order exponents from input $N(m,t)$ mass distribution data sets.

## 6.1 Our Results

As reported in Chapter 3, with the ambition of testing any new method against data sets that were as realistic as possible, we constructed (based on the method in Gillespie [1976]) Monte Carlo simulation software of the cluster-cluster aggregation process. This application was then used to generate $N(m,t)$ data sets containing noise arising from the stochastic nature of the simulation. It was found that there were two methods by which the level of noise could be approximately controlled: setting the size of an ensemble of runs that were averaged over; and tuning the number of particles within the system. While investigating the behaviour of the two regimes of behaviour of stationary solutions of the SCE, local

and nonlocal, two significant discoveries were made. In §3.4 we report our finding that for forward evolutions of a finite mass spectrum aggregation system with a source of mass injection using the "van Dongen" kernel with a sufficiently nonlocal parameterisation, collective oscillations of $N(m,t)$ solutions can persist in the presence of significant noise (see also Ball et al. [2012]). At a late stage in our research it was also discovered that for similar systems with kernel parameterisations that resulted in stable, but sensitive, nonlocal stationary solutions, the presence of noise in the system gave rise to behaviour indicative of phase-remembering, noise-driven quasicycles. Preliminary findings concerning the quasicycles are reported in §3.5. Both of these findings indicate that solution instabilities may persist as a result of inherent properties of real finite spectrum aggregration systems with a source and sink.

Equipped with both Monte Carlo and ODE simulation capabilities for generating test data sets, we then embarked on the main program of research into inverse methods. In Chapter 4 we showed that an existing inverse method [Wright and Ramkrishna, 1992] for use against scaling decay case distributions had marked limitations in respect of representing homogeneous kernels with fractional order exponents (see also Connaughton and Jones [2011]); and in Chapter 5 we demonstrated a new method that overcame most of these limitations. In particular, our novel use of a kernel factorisation has a powerful capacity to represent and retrieve homogeneous kernels with fractional order exponents from both stationary state and scaling decay case mass distribution data sets. In many cases it will retrieve an estimated kernel which almost exactly matches the true kernel. It also does not require extra methods for tuning regularisation, nor the extra minimisation iterations that such a process can require. As a result, the new method is also comparatively quick. As such, even at this stage of development, we believe that the new method offers significant progress in the pursuit of the wider research goals mentioned earlier.

## 6.2 Further Work

In order to obtain a complete picture of the full capabilities of the new method, some work remains to be done. At the time of writing, we have not yet been able to fully assess the response of our new method to the presence of significant noise in the input $N(m,t)$ distribution data. Since the method is already implicitly regularised by the use of a truncated Fourier series in the approximating kernel factorisation it is possible that results would not differ hugely from those demonstrated already. Proper assessment of the robustness of the method in this regard needs to be undertaken. The use of Bayesian approaches to inversion (see e.g. Stuart [2010]) may facilitate quantifying the error on the kernel function retrieved relative to input data noise levels.

It also remains to be seen whether the new method can be readily adjusted to work well with non-scaling, non-stationary $N(m,t)$ data. In this case homogeneity of the kernel cannot be presumed, and it may be necessary to revisit the question of reductive functional representations of general kernel functions in order to cater for the extra dimension of time.

Nevertheless, even in its current form our new method already improves the ability of researchers to use mass (density) distribution data to recover useful estimates of aggregation rate kernels.

# Appendix A

# Derivation of Eqn. 4 in Wright and Ramkrishna (1992)

As an informative aid, we provide here a derivation of Eqn. 4 in Wright and Ramkrishna [1992], which provides the basis for Eqn. 69 therein which is central to the inverse method presented in that paper. (We presume the validity of the mean-field approximation throughout.)

Given the equation for the cumulative mass fraction,

$$F(m,t) = \int_0^m \tilde{m} N(\tilde{m},t)\, d\tilde{m} \tag{A.1}$$

Then provided that $N(m,t)$ is not singular at either of the integral's limits we can take the time derivative inside the integral.

$$\frac{\partial F(m,t)}{\partial t} = \frac{\partial}{\partial t}\int_0^m \tilde{m} N(\tilde{m},t)\, d\tilde{m} = \int_0^m \tilde{m}\frac{\partial N(\tilde{m},t)}{\partial t} d\tilde{m} \tag{A.2}$$

We also know that the SCE (for the decay case) is,

$$\frac{\partial N(m,t)}{\partial t} = \frac{1}{2}\int_0^m K(m-m_1,m_1)N(m-m_1,t)N(m_1,t)\,dm_1 - \int_0^\infty K(m,m_1)N(m,t)N(m_1,t)\,dm_1 \tag{A.3}$$

Substituting the RHS of (A.3) in equation (A.2) gives,

$$\frac{\partial F(m,t)}{\partial t} = \int_0^m \tilde{m}\left[\frac{1}{2}\int_0^{\tilde{m}} K(\tilde{m}-m_1,m_1)N(\tilde{m}-m_1,t)N(m_1,t)\,dm_1 \quad (A) - \int_0^\infty K(\tilde{m},m_1)N(\tilde{m},t)N(m_1,t)dm_1\right] d\tilde{m} \quad (B) \tag{A.4}$$

Treating just term (B) on the RHS of (A.4), we have,

$$(B) = -\int_0^m \tilde{m}N(\tilde{m},t)\int_0^\infty K(\tilde{m},m_1)N(m_1,t)\,dm_1\,d\tilde{m} \tag{A.5}$$

$$= -\int_0^m \left[\int_0^{m-\tilde{m}} K(\tilde{m},m_1)N(m_1,t)\,dm_1 + \int_{m-\tilde{m}}^\infty K(\tilde{m},m_1)N(m_1,t)\,dm_1\right] dF(\tilde{m},t) \tag{A.6}$$

$$= -\int_0^m \int_0^{m-\tilde{m}} K(\tilde{m},m_1)\frac{dF(m_1,t)}{m_1}dF(\tilde{m},t) - \int_0^m \int_{m-\tilde{m}}^\infty K(\tilde{m},m_1)\frac{dF(m_1,t)}{m_1}dF(\tilde{m},t) \tag{A.7}$$

Treating term (A) on the RHS of (A.4), and making use of Iverson brackets, we have,

$$(A) = \int_0^m \int_0^{\tilde{m}} \frac{1}{2}\tilde{m}K(\tilde{m}-m_1,m_1)N(\tilde{m}-m_1,t)N(m_1,t)\,dm_1\,d\tilde{m} \tag{A.8}$$

$$= \iint_{-\infty}^{\infty} [0 \le \tilde{m} \le m][0 \le m_1 \le \tilde{m}]\,\frac{1}{2}\tilde{m}K(\tilde{m}-m_1,m_1)N(\tilde{m}-m_1,t)N(m_1,t)\,dm_1\,d\tilde{m} \tag{A.9}$$

Let $x = \tilde{m} - m_1$, $y = m_1, \Rightarrow \tilde{m} = x + y$, then,

$$(A) = \iint_{-\infty}^{\infty} [0 \le x+y \le m][0 \le y \le x+y]\,\frac{1}{2}(x+y)K(x,y)N(x,t)N(y,t)\,dy\,dx \tag{A.10}$$

$$= \iint_{-\infty}^{\infty} [0 \le x+y \le m][0 \le y][0 \le x]\,\frac{1}{2}(x)K(x,y)N(x,t)N(y,t)\,dy\,dx \tag{A.11}$$

$$+ \iint_{-\infty}^{\infty} [0 \le x+y \le m][0 \le y][0 \le x]\,\frac{1}{2}(y)K(x,y)N(x,t)N(y,t)\,dy\,dx$$

Assuming symmetry of the kernel, in the second integral in (A.11) we can map $(x,y) \to (y,x)$ and reverse the order of integrations, so that we can unite the two integrals and cancel the $1/2$. We then have,

$$(A) = \iint_{-\infty}^{\infty} [0 \le x+y \le m][0 \le y][0 \le x]\,xK(x,y)N(x,t)N(y,t)\,dy\,dx \tag{A.12}$$

$$= \iint_{0}^{\infty} [0 \le x+y \le m]\,K(x,y)\frac{dF(y,t)}{y}dF(x,t) \tag{A.13}$$

Reinstating the limits: $0 \le x+y \le m \Rightarrow 0 \le \tilde{m} - m_1 + m_1 \le m \Rightarrow 0 \le \tilde{m} \le m$ after substitution also implies $y \le m - \tilde{m} \Rightarrow m_1 \le m - \tilde{m}$. The resulting integral is then,

$$(A) = \int_0^m \int_0^{m-\tilde{m}} K(\tilde{m},m_1)\frac{dF(m_1,t)}{m_1}dF(\tilde{m},t) \tag{A.14}$$

The RHS of (A.14) then cancels with the first integral term in (A.7) and Eqn. 4 of [Wright and Ramkrishna, 1992] remains.

$$\frac{\partial F(m,t)}{\partial t} = -\int_0^m \int_{m-\tilde{m}}^{\infty} K(\tilde{m},m_1)\frac{dF(m_1,t)}{m_1}dF(\tilde{m},t) \tag{A.15}$$

# Appendix B

# Outline Derivations of Sample Kernel Functions

This appendix provides some background for the physical significance and derivations of the kernel functions mentioned in the main text. Kernel functions in the SCE model the essential physics (in the mean-field limit) of real aggregation processes. The underlying scheme common to these kernel functions is that they are proportional to the expectation of the probability that two particles, of masses $m_1, m_2$, with a given relative velocity will collide in time interval $dt$, and hence provide the (mean) rate of collision for a pair of masses when time is integrated out. Individual kernel functions then represent the application of this scheme to particular physical contexts.

The probability of collision is in turn a function of the radius of the relevant collision space (e.g. a volume or a cross-sectional area). Hence, when the physical derivations of kernels are stripped of their physical constants of proportionality, what remains is a product of some function of the collision space radius multiplied by an expression for the (average) relative velocity of the two particles. The relative velocity of the particles is determined by

the physical properties of the system.

The kernels in the main text are given solely in terms of masses. From the equation for a spherical mass in Euclidean $\mathbb{R}^3$ space, we have $m = \rho V$, where $\rho$ is the density and $V = \frac{4}{3}\pi R^3$ the volume of the sphere. Hence, the relationship between the mass and the radius of the sphere is given as:

$$m \propto R^3 \Rightarrow R \propto m^{1/3} \tag{B.1}$$

Hence if the collision space is given as a function $f(R) \propto R^x$, in mass terms we would have $\hat{f}(m) \propto m^{x/3}$.

Putting these parts together in respect of the scheme for kernel functions $K(m_1, m_2)$ outlined above: For some (physically appropriate) functions $\hat{f}_{\text{Coll}}$ and $\hat{g}_{\text{Vel}}$, we would expect an expression in terms of mass that resembled:

$$K(m_1, m_2) \propto \hat{f}_{\text{Coll}}(m_1, m_2)\hat{g}_{\text{Vel}}(m_1, m_2) \tag{B.2}$$

Taking this general model as a starting point, we can then discuss the kernel functions used in the thesis.

## B.1 Brownian Coagulation (Continuum Regime) Kernel

This kernel (first derived by Smoluchowski [1916]) represents the rate of coagulation of masses diffusing (in some continuous viscous medium) with random walks in Euclidean $\mathbb{R}^3$ space. Because, in the diffusive process, the two particles approach each other slowly

enough, the angle between their lines of approach to the collision is unimportant, but the geometry of the space in which the particles move can alter the rate at which they meet. In a $d$-dimensional space, the rate at which particles of diffusivity $D$ hit a sphere of radius $R$ is proportional to $DR^{d-2}$. Given two diffusing particles of radii $R_i$ and $R_j$, (for $d > 1$) the collision space is proportional to the sum $(R_i + R_j)^{d-2}$ [Krapivsky et al., 2010]. In $\mathbb{R}^3$, $d = 3$, and hence the collision space term is given by $(R_i + R_j)$.

The rate at which particles will diffuse into collisions is proportional to the sum of their diffusivities, $(D_i + D_j)$, which when multiplied by the collision space expression gives (in the mean-field limit):

$$K(i,j) \sim (R_i + R_j)(D_i + D_j) \tag{B.3}$$

From the Stokes-Einstein relationship between the diffusivity of a droplet, $D$, and the drag coefficient, $c_\delta = 6\pi\eta R$, given as $D = T/c_\delta$, where $T$ is system temperature and $\eta$ the kinematic viscosity of the medium, it is also the case that $D \propto m^{-1/3}$. Writing the kernel function solely in terms of mass then gives,

$$K_{\mathrm{BC}}(m_i, m_j) \sim (m_i^{1/3} + m_j^{1/3})(m_i^{-1/3} + m_j^{-1/3}) \tag{B.4}$$

A detailed contemporary derivation of this kernel for the specific context of the collision and aggregation of atmospheric aerosols can be found in Pruppacher and Klett [2010, Chapter 11].

Note that if the aggregating masses have fractal structure, with fractal dimension $d_f$, the relationship between mass and radius becomes,

$$m \propto R^{d_f} \Rightarrow R \propto m^{1/d_f} \tag{B.5}$$

With $\alpha = 1/d_f$ the Generalised Brownian Coagulation kernel is then given by,

$$K_{\mathrm{GBC}}(m_i, m_j) \sim (m_i^{\alpha} + m_j^{\alpha})(m_i^{-\alpha} + m_j^{-\alpha}) \tag{B.6}$$

## B.2 Saturn's Rings Kernel - Brownian Coagulation (Free Molecular Regime)

For the previous kernel in §B.1 two masses could diffuse toward each other and merge successfully irrespective of the directions from which the two particles came together. For the Saturn's Rings kernel, masses are presumed to be moving faster like ballistic projectiles, and therefore the relative angle of directions from which two masses can approach each other and merge successfully becomes important. If the angle between their lines of approach is too far away from $\theta = \pi$ then masses might just bounce off each other instead of aggregating. After averaging over the angles of attack suitable for successful collisions, the collision space becomes proportional to the cross-sectional area of a cylinder of interaction determined by the sum of the radii of two colliding masses: i.e. $\propto (R_i + R_j)^2$.

In the free molecular regime, where the masses behave like ballistic particles, the mean thermal velocity of a mass $m$ is the mean of the Maxwell-Boltzmann velocity distribution, given by,

$$\bar{v} = \sqrt{\frac{8k_B T}{\pi m}} \tag{B.7}$$

where $k_B$ is the Boltzmann constant of proportionality, and $T$ the temperature. The relative velocity expression in the kernel, $(v_i + v_j)$, is then assumed to take the form (see e.g. [Oh and Sorensen, 1997]),

$$(v_i + v_j) \propto \sqrt{\frac{1}{m_i} + \frac{1}{m_j}} \tag{B.8}$$

Combining this relative velocity expression with that of the collision space yields an expression for the kernel:

$$K_{\mathrm{SR}}(m_i, m_j) \sim (m_i^{1/3} + m_j^{1/3})^2 (m_i^{-1} + m_j^{-1})^{\frac{1}{2}} \tag{B.9}$$

## B.3 Differential Sedimentation Kernel

For the Differential Sedimentation kernel, masses are presumed to be moving in the same direction through a viscous medium in a field such that equal masses move with the same (mass dependent) velocity; for example when droplets fall at their terminal velocities through the atmosphere in a planet's gravitational field. Since the particles have to overlap to collide the collision space is therefore again proportional to the cross-sectional area of a cylinder of interaction determined by the sum of the radii of two colliding masses: i.e. $\propto (R_i + R_j)^2$.

The Stokes terminal velocity $v_z$ of a small sphere $s$ of radius $R$ (with no-slip boundary conditions) falling under the influence of gravity through the viscous medium $\varphi$ is given by,

$$v_z(R) = cR^2 \qquad c = \frac{2g(\rho_\varphi - \rho_s)}{9\eta} \tag{B.10}$$

where $g$ is the gravitational acceleration, $\rho_\varphi$ is the density of the viscous medium with kinematic viscosity $\eta$, and $\rho_s$ is the density of the sphere [Horvai et al., 2008]. Larger spheres fall faster than smaller ones, and since the relative velocity towards collision depends on which falling mass we choose to fix for the frame of reference, from ruling out the possible asymmetry it becomes $|v(R_1) - v(R_2)|$.

Combining the collision space and velocity expressions in terms of mass gives:

$$K_{\mathrm{DS}}(m_i, m_j) \sim (m_i^{1/3} + m_j^{1/3})^2 |m_i^{2/3} - m_j^{2/3}| \tag{B.11}$$

## B.4 Shear (Nonlinear Velocity Profile) Kernel

This variant of a shear kernel arises from considering the collision rates of droplets in a turbulent flow [Shiloh et al., 1973][Tobin et al., 1990] such as impeller driven chemical batch mixing in reactor vessels. It may also have relevance for the study of raindrop coalescence in clouds. The collision space is again $(m_i^{1/3} + m_j^{1/3})^2$. The relative velocity term is derived from the root mean square relative velocity fluctuation $|\bar{v}|$, which for particles larger than the Kolmogorov dissipation length is estimated to be,

$$|\vec{v}| \propto (R_1 + R_2)^{1/3} \tag{B.12}$$

Multiplying these factors together and expressing them in terms of mass, gives the kernel,

$$K_{\mathrm{SNLV}}(m_i, m_j) \sim (m_i^{1/3} + m_j^{1/3})^{7/3} \tag{B.13}$$

## B.5 Sum Kernel

This kernel is relevant to the turbulent coagulation of colloids [Tobin et al., 1990], pre-planetary gravitational accretion scenarios [Hallam and Marcus, 1974], and cloud droplet coalescence [Scott, 1968]. Generalisations exist for other scenarios, including coagulation during epitaxial film deposition [Krapivsky et al., 2010, Ch. 5]. It is typically derived as an approximation to specific scenarios.

## B.6 Constant Kernel

In physical problems the constant kernel, $K(m_1, m_2) = C$ (where $C$ is a scalar constant, often normalised to $C = 1$), arises partly as a gross approximation because the Brownian Coagulation kernel has degree of homogeneity zero, implying the invariance $K(am_1, am_2) = K(m_1, m_2)$ [Krapivsky et al., 2010]. However, for the Brownian Coagulation kernel it is clearly the case that $K(m_1, m_2) \neq K(m_1, m_3)$ when $m_2 \neq m_3$. So strictly speaking, the constant kernel represents aggregation rates that are entirely independent of mass. This is rigorously justifiable in more abstract settings, such as problems concerning 'lines of descent' in mathematical population genetics [Tavare, 1984].

## B.7 “van Dongen” Kernel

This kernel,

$$K_{\mathrm{VD}}(m_i, m_j) = \frac{1}{2}(m_i^{\mu} m_j^{\nu} + m_i^{\nu} m_j^{\mu}) \tag{B.14}$$

appeared in works investigating the analysis of solutions of the SCE [van Dongen, 1987a; van Dongen and Ernst, 1988]. It is a model for a class of kernels that permits the analysis of the behaviour of solutions for large times when $K_{\mathrm{VD}}(m_i, m_j) \sim m_i^{\mu} m_j^{\nu}$ with $m_i \ll m_j$. It has degree of homogeneity $\lambda = \mu + \nu$. For the special case $\mu = \nu = 0$ it represents the constant kernel. Similarly, when $\mu = 0, \nu > 0$ (or vice versa), it represents the sum kernels.

# Bibliography


D. J. Aldous. Deterministic and stochastic models for coalescence (aggregation and coagulation): a review of the mean-field theory for probabilists. *Bernoulli*, **5**:3–48, 1999.

R. C. Aster, B. Borchers, and C. H. Thurber. *Parameter Estimation and Inverse Problems*. Elsevier Academic Press, 2005.

R. C. Ball, C. Connaughton, T. H. M. Stein, and O. Zaboronski. Instantaneous gelation in the Smoluchowski coagulation equation revisited. *Phys. Rev. E*, **84**:011111, 2011.

R. C. Ball, C. Connaughton, P. P. Jones, R. Rajesh, and O. Zaboronski. Collective Oscillations in Irreversible Coagulation Driven by Monomer Inputs and Large-Cluster Outputs. *Phys. Rev. Lett.*, **109**:168304, 2012.

M. S. Bartlett. Measles periodicity and community size. *J. Royal. Stat. Soc. A*, **120**:48–70, 1957.

F. Bauer and M. A. Lukas. Comparing parameter choice methods for regularization of ill-posed problems. *Mathematics and Computers in Simulation*, **81**:1795–1841, 2011.

J. Bertoin. *Random Fragmentation and Coagulation Processes*, volume 102 of *Cambridge Studies in Advanced Mathematics*. Cambridge, 2006.

E. Bodenschatz, S. P. Malinowski, R. A. Shaw, and F. Stratmann. Can We Understand Clouds Without Turbulence? *Science*, **327**(5968):970–971, 2010.

R. P. Boland, T. Galla, and A. J. McKane. How limit cycles and quasi-cycles are related in systems with intrinsic noise . *Journ. of Stat. Mech.: Theory and Experiment*, page P09001, 2008.

R. P. Boland, T. Galla, and A. J. McKane. Limit cycles, complex Floquet multipliers, and intrinsic noise. *Phys. Rev. E*, **79**:051131, 2009.

N. V. Brilliantov, A. S. Bodrova, and P. L. Krapivsky. A model of ballistic aggregation and fragmentation. *Journ. of Stat. Mech.: Theory and Experiment*, page P06011, 2009.

Y. Cao, H. Li, and L. Petzold. Efficient Formulation of the Stochastic Simulation Algorithm for Chemically Reacting Systems. *J. Chemical Physics*, **121**(9):4059–4067, 2004.

C. Connaughton and P. P. Jones. Some Remarks on the Inverse Smoluchowski Problem for Cluster-Cluster Aggregation. In *J. Phys.: Conf Ser.*, number 012005 in 333, 2011. doi: 10.1088/1742-6596.

C. Connaughton, R. Rajesh, and O. Zaboronski. Stationary Kolmogorov Solutions of the Smoluchowski Aggregation Equation with a Source Term. *Phys. Rev. E*, **69**(6):061114, 2004.

C. Connaughton, R. Rajesh, and O. Zaboronski. Cluster–cluster aggregation as an analogue of a turbulent cascade: Kolmogorov phenomenology, scaling laws and the breakdown of self-similarity. *Physica D*, **222**:57–115, 2006.

C. Connaughton, R. Rajesh, and O. Zaboronski. Constant flux relation for diffusion-limited cluster-cluster aggregation. *Phys. Rev. E*, **78**:041403, Oct 2008.

C. Connaughton, R. Rajesh, and O. Zaboronski. *Handbook of Nanophysics*, chapter Kinetics of Cluster-Cluster Aggregation. 2009.

A. Costa, A. Folch, and G. Macedonio. A model for wet aggregation of ash particles in volcanic plumes and clouds: 1. Theoretical formulation. *Journal of Geophysical Research*, **115**:B09201, 2010.

J. G. Crump and J. H. Seinfeld. On Existence of Steady-State Solutions to the Coagulation Equations. *J. Colloid Interface Science*, **90**(2):469, 1982.

S. C. Davies, J. R. King, and J. A. D. Wattis. Self-similar behaviour in the coagulation equations. *Journal of Engineering Mathematics*, **36**:57–88, 1999.

B. J. Devenish, P. Bartello, J.-L. Brenguier, L. R. Collins, W. W. Grabowski, R. H. A. IJzermans, S. P. Malinowski, M. W. Reeks, J. C. Vassilicos, L.-P. Wang, and Z. Warhaft. Droplet growth in warm turbulent clouds. *Quarterly Journal of the Royal Meteorological Society*, 2012. ISSN 1477-870X.

A. Doicu, T. Trautmann, and F. Schreier. *Numerical Regularization for Atmospheric Inverse Problems*. Springer, 2010.

C. A. Dorao and H. A. Jakobsen. A Least-Squares Method for the Solution of Population Balance Problems. *Computers and Chemical Engineering*, **30**:535–547, 2006.

M. Escobedo and S. Mischler. Dust and self-similarity for the Smoluchowski coagulation equation. *Annales de l'Institut Henri Poincare (C) Non Linear Analysis*, **23**(3):331–362, 2006. ISSN 0294-1449.

G. Falkovich, A. Fouxon, and M. G. Stepanov. Acceleration of rain initiation by cloud turbulence. *Nature*, **419**:151–154, 2002.

N. Fournier and J.-S. Giet. Convergence of the Marcus-Lushnikov process. *Methodology and Computing in Applied Probability*, **6**:219–231, 2004.

N. Fournier and P. Laurençot. Existence of Self-Similar Solutions to Smoluchowski's Coagulation Equation. *Commun. Math. Phys.*, **256**:589–609, 2005.

S. K. Friedlander. *Smoke, Dust and Haze*. New York: Wiley Interscience, 1977.

M.A. Gibson and J. Bruck. Efficient Exact Stochastic Simulation of Chemical Systems with Many Species and Many Channels. *J. Physical Chemistry A*, **104**(9):1876–1889, 2000.

D. T. Gillespie. A General Method for Numerically Simulating the Stochastic Time Evolution of Coupled Chemical Reactions. *Journal of Computational Physics*, **22**:403–434, 1976.

D.T. Gillespie. Stochastic Simulation of Chemical Kinetics. *Ann. Rev. of Physical Chemistry*, **58**:35–55, 2007.

J. Goodisman and J. Chaiken. Scaling and the Smoluchowski equations. *The Journal of Chemical Physics*, **125**:074304, 2006.

W. W. Grabowski and L.-P. Wang. Diffusional and accretional growth of water drops in a rising adiabatic parcel: effects of the turbulent collision kernel . *Atmos. Chem. Phys.*, **9**: 2335–2353, 2009.

W. C. S. Gurney and R. M. Nisbet. *Ecological dynamics*. Ox. Univ. Press, 1998.

M. Hallam and A. H. Marcus. Stochastic Coalescence Model for Terrestrial Planetary Accretion. *Icarus*, **21**:66–85, 1974.

P. C. Hansen. The L-curve and its use in the numerical treatment of inverse problems. In P. Johnston, editor, *Computational Inverse Problems in Electrocardiology*, pages 119–142. WIT Press, 2001.

H. Hayakawa. Irreversible kinetic coagulations in the presence of a source. *J. Phys. A: Math. Gen.*, **20**:L801–L8O5, 1987.

E. M. Hendriks and R. M. Ziff. Coagulation in a Continuously Stirred Tank Reactor. *J. Colloid Interface Science*, **105**(1):247, 1985.

P. Horvai, S. V. Nazarenko, and T. H. M. Stein. Coalescence of Particles by Differential Sedimentation. *J. Stat. Phys.*, **130**:1177–1195, 2008.

K. Kang, S. Redner, P. Meakin, and F. Leyvraz. Long-time crossover phenomena in coagulation kinetics. *Phys. Rev. A*, **33**(2):1172–1182, 1986.

P. L. Krapivsky and C. Connaughton. Driven Brownian coagulation of polymers. *J. Chem. Phys.*, **136**:204901, 2012.

P. L. Krapivsky, S. Redner, and E. Ben-Naim. *A Kinetic View of Statistical Physics*. Cambridge University Press, 1st edition, 2010.

M.H. Lee. On the validity of the coagulation equation and the nature of runaway growth. *Icarus*, **143**:74–86, 2000.

F. Leyvraz. Scaling theory and exactly solved models in the kinetics of irreversible aggregation. *Phys. Reports*, **383**(2):95–212, Aug 2003.

H. Li and L. Petzold. Logarithmic Direct Method for Discrete Stochastic Simulation of Chemically Reacting Systems. Technical report, Dept. of Computer Science, Univ. of California, Santa Barbara, 2006. URL `http://www.engr.ucsb.edu/~cse`.

A. A. Lushnikov. Gelation in coagulating systems. *Physica D*, **222**:37–53, 2006.

K. Mallick and P. Marcq. Stability analysis of a noise-induced Hopf bifurcation. *Eur. Phys. Jour. B*, **36**:119–128, 2003.

S. Mauch and M. Stalzer. Efficient Formulations for Exact Stochastic Simulation of Chemical Systems. *IEEE/ACM Transactions on Computational Biology and Bioinformatics*, **8**(1):27–35, 2011.

J.M. McCollum, G.D. Peterson, C.D. Cox, M.L. Simpson, and N.F. Samatova. The Sorting Direct Method for Stochastic Simulation of Biochemical Systems with Varying Reaction Execution Behavior. *Computational Biology and Chemistry*, **30**(1):39–49, 2006.

A. J. McKane and T. J. Newman. Predator-Prey Cycles from Resonant Amplification of Demographic Stochasticity. *Phys. Rev. Lett.*, **94**:218102, Jun 2005.

G. Menon and R. L. Pego. Approach to Self-Similarity in Smoluchowski's Coagulation Equations. *Comms. on Pure and Applied Mathematics*, **57**:1197–1232, 2004.

G. Menon and R. L. Pego. Dynamical Scaling in Smoluchowski's Coagulation Equations: Uniform Convergence. *SIAM Review*, **48**(4):745–768, 2006.

G. Menon and R. L. Pego. The Scaling Attractor and Ultimate Dynamics for Smoluchowski's Coagulation Equations. *Journal of Nonlinear Science*, **18**:143–190, 2008.

M. Mobilia, I. T. Georgiev, and U. C. Täuber. Phase Transitions and Spatio-Temporal Fluctuations in Stochastic Lattice Lotka–Volterra Models. *Journal of Statistical Physics*, **28**(1/2):447, 2007.

S. Morita, Y. Itoh, and K. Tainaka. Frequency of Stochastic Oscillations in Interacting Population Models. *Journ. of Phys. Soc. of Japan*, **74**(3):819–822, 2005.

H. Müller. Zur algemeinen Theorie der raschen Koagulation. *Kolloidchemische Beihefte*, **27**:223, 1928.

R. Muralidhar and D. Ramkrishna. An inverse problem in agglomeration kinetics. *J. Colloid Interface Science*, **112**(348), 1986.

R. Muralidhar and D. Ramkrishna. Inverse problems of agglomeration kinetics: II. Binary clustering coefficients from self-preserving spectra. *J. Colloid Interface Science*, **131** (503), 1989.

R. M. Nisbet and W. C. S. Gurney. A simple mechanism for population cycles. *Nature*, **263**:319–320, 1976.

R. M. Nisbet and W. C. S. Gurney. *Modeling Fluctuating Populations*. WIley, 1982.

J. R. Norris. Smoluchowski's coagulation equation: uniqueness, nonuniqueness and a hydrodynamic limit for the stochastic coalescent. *Ann. Appl. Probab.*, **9**:78–109, 1999.

C. Oh and C. M. Sorensen. Light Scattering Study of Fractal Cluster Aggregation Near the Free Molecular Regime. *J. Aerosol Science*, **28**(6):937–957, 1997.

R. Onishi, K. Matsuda, K. Takahashi, R. Kurose, and S. Komori. Retrieval of collision kernels from the change of droplet size distributions with a simple inversion scheme. *Phys. Scr.*, **T132**:014050, 2008.

R. Onishi, K. Matsuda, K. Takahashi, K. Ryoichi, and S. Komori. Linear and nonlinear inversion schemes to retrieve collision kernel values from droplet size distribution change. *Int. J. Multiphas. Flow*, **37**:125–135, 2011.

O. P. Prat and A. P. Barros. A Robust Numerical Solution of the Stochastic Collection–Breakup Equation for Warm Rain. *Journal of Applied Meteorology and Climatology*, **46**: 1480–2014, 2007.

H. R. Pruppacher and J. D. Klett. *Microphysics of Clouds and Precipitation*. Springer, 2nd edition, 2010. ISBN 978-0-7923-4211-3.

W. C. Reade and L. R. Collins. A numerical study of the particle size distribution of an aerosol undergoing turbulent coagulation. *J. Fluid Mech.*, **415**:45–64, 2000.

E. Renshaw. *Modelling biological populations in space and time*. Cambridge Univ. Press, 1991.

R. R. Rogers and M. K. Yau. *A Short Course In Cloud Physics*. Butterworth Heinemann, 3rd edition, 1989.

W. T. Scott. Analytic Studies of Cloud Droplet Coalescence I. *Journal of Atmospheric Sciences*, **25**:54–65, 1968.

K. Shiloh, S. Sideman, and W. Resnick. Coalescence and break-up in dilute polydispersions. *The Canadian Journal of Chemical Engineering*, **51**(5):542–549, 1973.

I. A. Shuda, S. S. Borysov, and A. I. Olemskoi. Noise-induced oscillations in non-equilibrium steady state systems. *Phys. Scr.*, **79**:065001, 2009.

H. Siebert, K. Lehmann, M. Wendisch, H. Franke, R. Maser, D. Schell, E. Wei Saw, and R. A. Shaw. Probing Finescale Dynamics and Microphysics of Clouds with Helicopter-Borne Measurements. *Bull. Am. Meteorol. Soc.*, **87**(12):1727–1738, 2006.

J. Silk and S. D. White. The development of structure in the expanding universe. *Astrophys. J.*, **223**:L59–L62, 1978.

A. Slepoy, A.P. Thompson, and S.J. Plimpton. A Constant-Time Kinetic Monte Carlo Algorithm for Simulation of Large Biochemical Reaction Networks. *J. Chemical Physics*, **128**(205101), 2008.

D. J. Smit, M. J. Hounslow, and W. R. Paterson. Aggregation and Gelation - I. Analytical Solutions for CST and Batch Operation. *Chemical Engineering Science*, **49**(7):1025–1035, 1994.

M. V. Smoluchowski. Drei Vorträge über Diffusion, Brownsche Bewegung und Koagulation von Kolloidteilchen. *Physik. Z.*, **17**:557–585, 1916.

M. V. Smoluchowski. Versuch einer mathematischen Theorie der Koagulationskinetik kolloider Lösungen. *Z. Phys. Chem.*, **91**:129, 1917.

J. L. Spouge. Solutions and critical times for the monodisperse coagulation equation when $a(i,j) = A + B(i+j) + Cij$. *J. Phys. A: Math. Gen.*, **16**:767–773, 1983a.

J. L. Spouge. Solutions and critical times for the polydisperse coagulation equation when $a(x,y) = A + B(x+y) + Cxy$. *J. Phys. A–Math. Gen.*, **16**:3127–3132, 1983b.

G. L. Stephens. Cloud Feedbacks in the Climate System: A Critical Review. *J. Climate*, **18**:237–273, 2005.

A. M. Stuart. Inverse problems: A Bayesian Perspective. *Acta Numerica*, **19**:451–559, 2010.

S. Tavare. Line-of-descent and genealogical processes and their applications in population genetics models. *Theoretical Population Biology*, **263**:119–164, 1984.

T. Tobin, R. Muralidhar, H. Wright, and D. Ramkrishna. Determination of Coalescence Frequencies in Liquid-Liquid Dispersions: Effect of Drop Size Dependence. *Chemical Engineering Science*, **45**(12):3491–3504, 1990.

T. Tomé and M. J. de Oliveira. Role of noise in population dynamics cycles. *Phys. Rev. E*, **79**:061128, 2009.

P. G. J. van Dongen. Solutions of Smoluchowski's Coagulation Equation at Large Cluster Sizes. *Physica A*, **145**:15–66, 1987a.

P. G. J. van Dongen. Fluctuations in Coagulating Systems. II. *J. Stat. Phys.*, **49**(5):927–975, 1987b.

P. G. J. van Dongen and M. H. Ernst. On the occurrence of a gelation transition in Smoluchowski's coagulation equation. *J. Stat. Phys.*, **44**:785, 1986.

P. G. J. van Dongen and M. H. Ernst. Scaling Solutions of Smoluchowski's Coagulation Equation. *Journal of Statistical Physics*, **50**(1/2):295–329, 1988.

N. G. van Kampen. *Stochastic Processes in Physics and Chemistry*. Elsevier Academic Press, 3rd edition, 2007.

L.-P. Wang, O. Ayala, B. Rosa, and W. W. Grabowski. Turbulent collision efficiency of heavy particles relevant to cloud droplets. *New J. Phys.*, **10**(7):075013, 2008.

J. A. D. Wattis. An introduction to mathematical models of coagulation–fragmentation processes: A discrete deterministic mean-field approach. *Physica D*, **222**:1–20, 2006.

W. H. White. On the Form of Steady-State Solutions to the Coagulation Equations. *J. Colloid Interface Science*, **87**(1):204, 1982.

H. Wright and D. Ramkrishna. Solutions of Inverse Problems in Population Balances - I. Aggregation Kinetics. *Computers Chem. Eng.*, **16**(12):1019–1038, 1992.

H. Wright, R. Muralidhar, T. Tobin, and D. Ramkrishna. Inverse problems of aggregation processes. *J. Stat. Phys.*, **61**(843), 1990.

H. Wright, R. Muralidhar, and D. Ramkrishna. Aggregation Frequencies of Fractal Aggregation. *Phys. Rev. A*, **46**(8):5072–5083, October 1992.

C. Xiao and A. O. Ling. Accelerated Stochastic Simulation of Large Chemical Systems. *Chinese Phys. Lett.*, **24**:2509–2513, 2007.

V. Zakharov, V. Lvov, and G. Falkovich. *Kolmogorov Spectra of Turbulence*. Springer-Verlag, 1992.